To the Graduate Council:

I am submitting herewith a thesis written by Nancy Diane O'Brien entitled "Effect of Liquid Rocket Coaxial Fuel Injector Distributions on Combustion Efficiency." I have examined the final copy of this thesis for form and content and recommend that it be accepted in partial fulfillment of the requirements for the degree of Master of Science with a major in Aerospace Engineering.

Roy J. Schulz

Dr. Roy J. Schulz, Major Professor

We have read this thesis and recommend its acceptance:

Roger Crawford

Accepted for the Council:

Associate Vice Chancellor
and Dean of The Graduate School

STATEMENT OF PERMISSION TO USE

In presenting this thesis in partial fulfillment of the requirements for a Master's degree at The University of Tennessee, Knoxville, I agree that the Library shall make it available to borrowers under rules of the Library. Brief quotations from this thesis are allowable without special permission, provided that accurate acknowledgement of the source is made.

Permission for extensive quotation from or reproduction of this thesis may be granted by my major professor, or in his absence, by the Head of the Interlibrary when, in the opinion of either, the proposed use of the material is for scholarly purposes. Any copying or use of the material in this thesis for financial gain shall not be allowed without my written permission.

Signature: Nancy Diane O'Bri

Date: 5/25/93

Effect of Liquid Rocket Coaxial Fuel Injector Distributions on Combustion Efficiency

A Thesis

Presented for the

Master of Science

Degree

The University of Tennessee, Knoxville

Nancy Diane O'Brien

August, 1993

ACKNOWLEDGEMENTS

I would like to thank my major professor, Dr. Roy J. Schulz, for his patience and guidance during my entire Master's program. I would also like to thank my parents for the love and support they have given me writing this thesis, and in everything that I have done.

ABSTRACT

This thesis is a qualitative analysis of various liquid rocket motor coaxial element fuel injector patterns, and their effect on combustion efficiency. The Performance/Life Combustion (PLC) Model, a computer program that analyzes gaseous fuel-liquid oxidizer combustion chambers, was used for the study. PLC is a submodel of the liquid rocket motor design code ROCket Combustor Interactive Design (ROCCID) Model.

Modifications were made to PLC to improve its modelling procedures. Output from various injector layouts are presented in the form of tabulated values of combustion efficiency, and color plots of mixture ratio distributions at the throat of a combustion chamber. The data are analyzed and recommendations for future work are made.

TABLE OF CONTENTS

LIST OF FIGURES

CHAPTER ONE

INTRODUCTION

The choice of a liquid-fueled rocket engine injector layout is often based on experience and empirical data. This thesis is a qualitative analysis of various injector patterns, and their effects on combustion efficiency and chamber pressure. Patterns are analyzed computationally, and comparisons made based on the output of a research and design program for liquid rocket motors[1]. Computer programs can save both time and money by predicting the effect of injector variations. Poorly performing configurations can be eliminated from consideration without the expense of actually building a test model. The ROCket Combustor Interactive Design (ROCCID) and Analysis computer program[1] was developed by Lewis Research Center for this purpose.

ROCCID analyzes the performance and combustion stability of a rocket, and is also capable of designing a stable, high performance thruster to meet a given set of design parameters. ROCCID's performance analysis program predicts a combustor's steady state performance, low-frequency (or chug) stability, and high-frequency (or acoustic) stability. ROCCID accepts both liquid/liquid and gas/liquid fuel-oxidizer injection. It can also calculate the properties for most traditional propellants. ROCCID provides a selection of injector geometries (including showerhead, doublet, triplet, shear coaxial and swirl coaxial injectors). ROCCID also models Helmholtz resonators, radial thrust chamber baffles, acoustic cavities and predicts their effects on combustion stability.[1]

In the original intent of this thesis research, ROCCID was to be used to model an oxygen gas generator, a combustor operating at very high mixture ratios (O/F≈100/1). Such combustors could be used to drive the turbine of a liquid oxygen turbopump[2]. The gas generator configuration being studied consisted of a long cylindrical combustion chamber, and a single coaxial injector comprised of an annular oxidizer and core fuel stream (See Figure 1).

One primary difficulty in using ROCCID to analyze the generator involved modelling the injector configuration. ROCCID provides a shear coaxial element, but does not allow for the fuel/oxidizer arrangement required by the oxygen gas generator. ROCCID only models an annular fuel, central oxidizer injector.[1] Because the needed element was not available in ROCCID, modifications to the program would be required.

Before any modifications were made to ROCCID, the program's performance was studied by running some cases using the type of coaxial injector element included in the program. There were problems with mass flow convergence. Mass flows calculated by ROCCID never matched design predictions. The Low Frequency Combustion Stability model predicted very high chug instability pressures (6000-6500 psia), and the High Frequency Combustion Stability model never ran without error for even sample cases. These problems were not resolved, and communications with NASA engineers indicated that similar difficulties have been noted in other applications.

In order to modify ROCCID to accept the oxygen gas generator injector configuration, an in-depth analysis of ROCCID's subroutines was

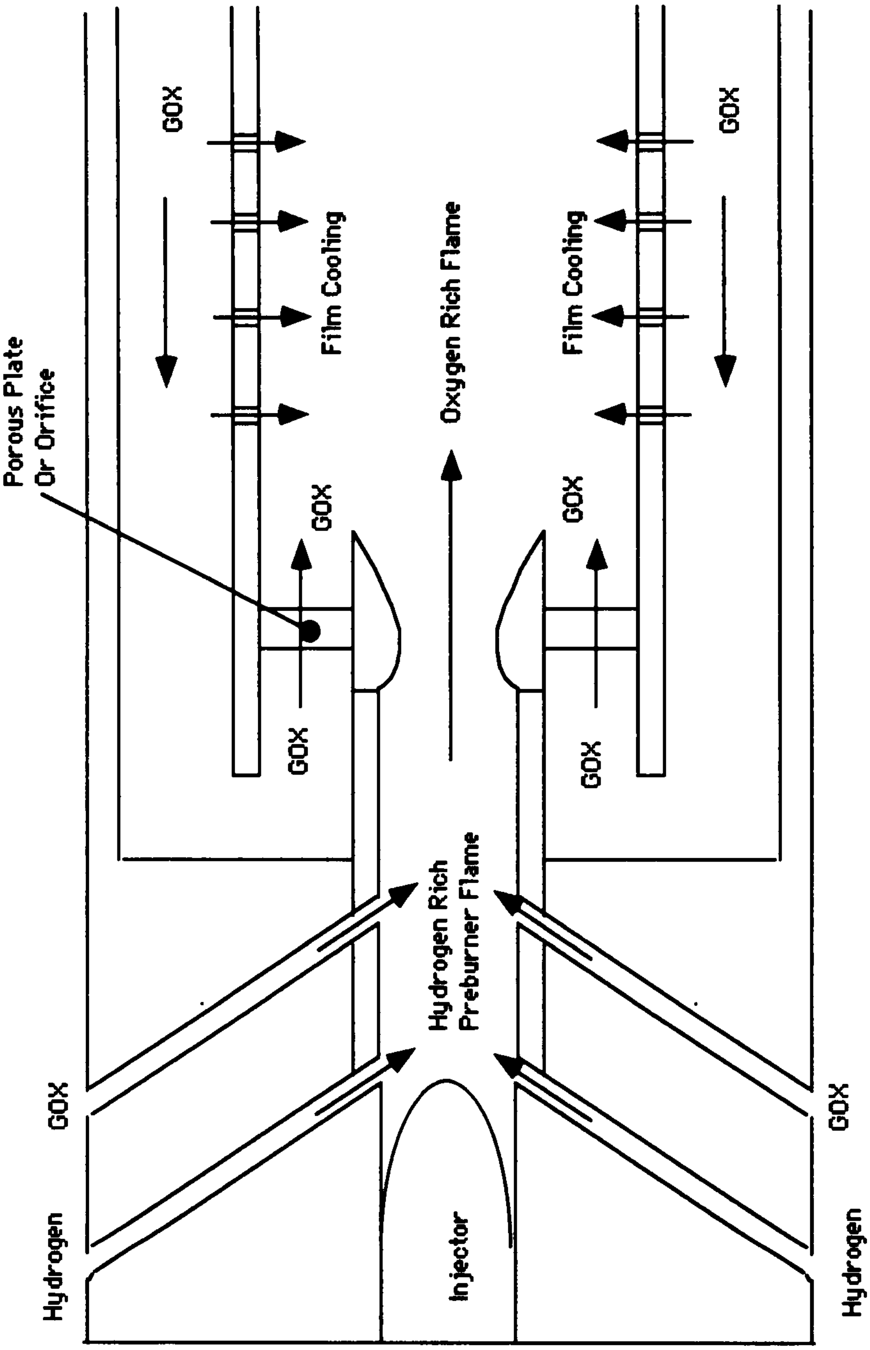

Figure 1. Oxygen gas generator configuration

Source: Paul Wayne Gloyer, "A Preliminary Study of Oxygen Rich Combustion Gas Generator Technology for Lox Tank Pressurization." Master of Science Thesis in Aerospace Engineering, The University of Tennessee, Knoxville, May 1993.

required, especially those routines responsible for the atomization and vaporization of the liquid propellants. Examination of reference material[3] for these routines led the author to study the Performance/Life Combustion (PLC) Model, a subprogram that is the basis of ROCCID's atomization/vaporization routines. PLC was originally written to analyze the wall mixture ratios, and energy release efficiency of the Space Shuttle Main Engine. This information was to be used along with structural, thermal, and performance models to evaluate the overall performance and life expectancy of the thrust chamber.[3]

PLC models a gaseous fuel-liquid oxidizer rocket combustor with shear coaxial injectors. PLC's primary purpose is to model the atomization and vaporization of a liquid oxidizer stream, and track the movement of the droplets and propellant vapor throughout the chamber.[3] While PLC does not incorporate all of the physical processes considered by ROCCID, it does provide a basic analysis of how the atomization and vaporization processes develop in the chamber. Therefore, it was concluded that PLC is the submodel that essentially predicts the steady-state combustion efficiency of the thrust chamber, as well as the chamber pressure. Further, PLC could, in principle, be used to determine the effects of liquid rocket fuel injector element distribution patterns, across the face of the injector plate, or the combustion efficiency and chamber pressure. PLC could serve as a basis for a method of screening injector distributions or patterns to identify those that give good performance. Therefore, the purpose of the thesis research was refocussed on an analysis of the existing methodology in PLC used to predict combustor energy release efficiency and chamber pressure, and to improve it, if necessary. Then, PLC would be used to prepare a preliminary study of the effects of injector element patterns (number of elements, and their geometrical arrangements) on combustion heat release efficiency and chamber pressure. From this, some "good" and some "poor" patterns might be identified.

This type of information, and an improved PLC subprogram, could provide extremely useful tools for design and evaluation of liquid fueled thrust chambers for gas generators and rocket motors.

CHAPTER TWO

PERFORMANCE/LIFE COMBUSTION MODEL

Introduction to PLC

The primary mission of the Performance/Life Combustion (PLC) program is to monitor the flow development from injector plate to nozzle throat in a liquid rocket combustion chamber. The program assumes gaseous hydrogen and liquid oxygen as propellants and shear coaxial injectors[4]. PLC models a axisymmetric combustion chamber from the injector plate to the nozzle throat.

PLC follows liquid oxidizer streams from injection to atomization. Once atomization begins, the program begins to move and vaporize the oxidizer droplets. When the flow reaches the nozzle throat, an "energy release efficiency" and the percentage of liquid oxidizer vaporized are calculated.

Programming Logic of PLC Code

PLC makes many assumptions to simplify its calculations. The program assumes that in an area close to the injector plate the flow is contained in streamtubes, and that downstream the flow can be modeled with grid cells. PLC discretizes the flow with a grid structure that divides the chamber into finite volumes (See Figure 2). The grid is constructed with radial "slices" and circular "segments." The number of slices and segments depends on the number of injectors and the number of injector rings.

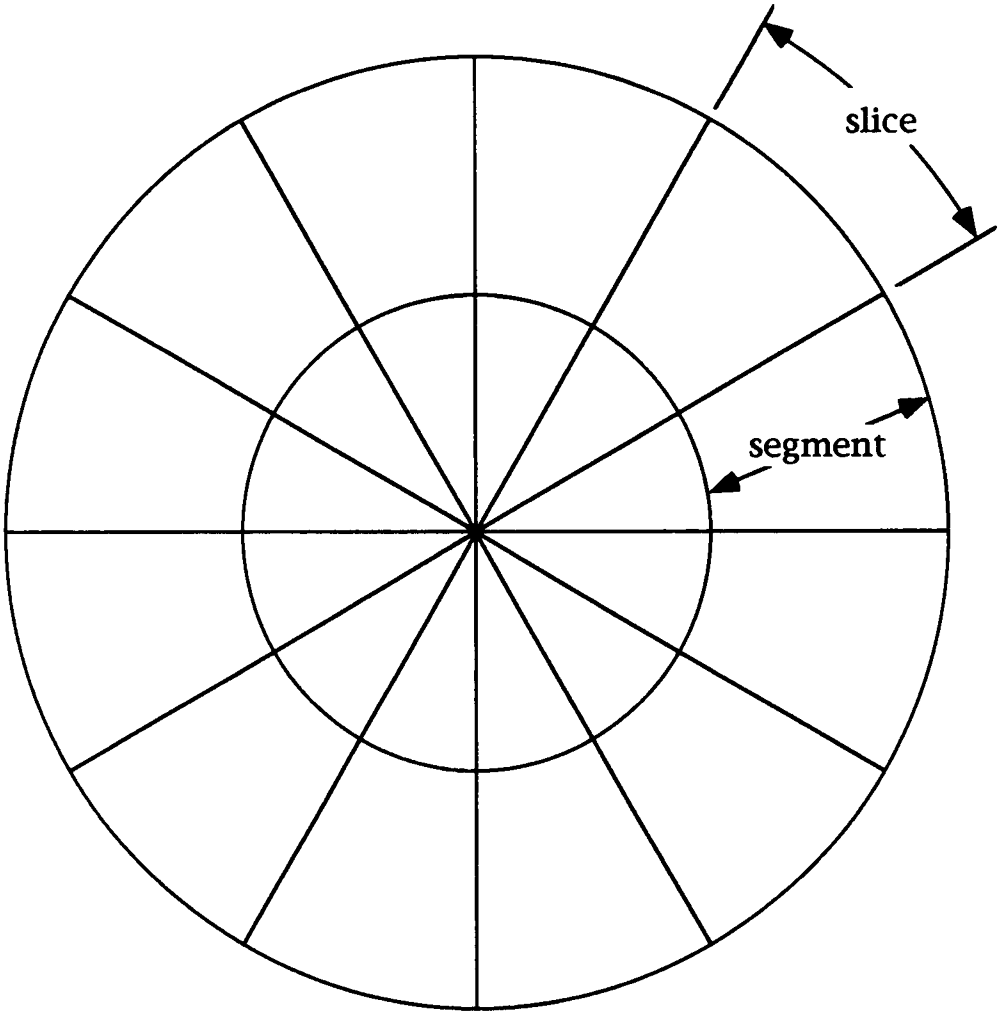

Figure 2. PLC grid structure.

$$N_{slice} = \begin{cases} N_{inj} - 1 & if \quad N_{rows} = 1 \; \& \; N_{inj} \leq 13 \\ 12 \end{cases} \qquad (1)$$

$$N_{seg} = N_{rows} + 1 \qquad (2)$$

where N_{slice} = number of radial slices,

N_{inj} = number of injectors,

N_{rows} = number of rings of injectors,

N_{seg} = number of circular segments.

These slice/segments are sized to create cells of equal area. For any axial cross-section, the number of grid cells is constant, but the cell area changes with the cross-sectional area.

Pressure is assumed to be equal to a nominal chamber pressure (an initial input parameter) and constant for any cross-section in the cylindrical portion of the combustion chamber. Vapor in the grid cells is assumed to be well mixed and the gas properties for each cell (ratio of specific heats(γ), molecular weight, static temperature, sonic velocity, density, characteristic exhaust velocity (C*), and dynamic viscosity) are based on the vapor mixture ratio and pressure in that cell, and one-dimensional chemical equilibrium property tables generated by the Two-Dimensional Kinetic Reference Computer Program.[5] PLC calculates the gas properties using a routine that interpolates tabulated properties, valid over a range of mixture ratios of 0-20 and pressures of 300-3000 psia. For values outside the range of the tables, the table values are extrapolated.

Droplet volume is assumed to be insignificant, so the vapor fills the cross-section. Droplets are also assumed to have no drag effect on the vapor flow, but the vapor is assumed to accelerate the droplets. It is assumed that droplets move in evenly distributed rings centered on the injector axis and vapor from the droplets is assumed to be uniformly distributed around the droplet position.[3]

PLC's first step is to read in propellant properties, chamber geometry, injector location and dimensions, and mass flow rates. The grid structure is generated using this data, and the program then begins to model the development of the flow from the injector plate downstream. The first step is to model the atomization of the liquid oxidizer element core flow. The atomization model begins by calculating all possible drop sizes that will be created. At any axial location, for a given liquid oxidizer core radius, only a single drop size is computed, but this drop size changes (decreases) as the cone jet radius is reduced, axially, by the shear-stripping atomization process. Drop sizes are calculated by

$$r_m = \frac{8 \cdot ST}{\tau \cdot g_c} \tag{3}$$

where r_m = the droplet radius in ft,

ST = the oxidizer surface tension in lb_f/ft,

τ = the interfacial shear stress in $lb_m/ft\text{-}sec^2$,

g_c = 32.2 (ft lb_m)/(lb_f sec^2).

The interfacial shear stress, τ, is estimated by

$$\tau = \frac{\mu_m \left(v_f - v_{ox} \right)}{t_{post} + \Delta r_{jet}} \tag{4}$$

where μ_m = the mean dynamic viscosity in lb_m/ft-sec,

v_f = the fuel velocity in ft/sec,

v_{ox} = the oxidizer free surface velocity in ft/sec,

t_{post} = the injector oxidizer post wall thickness in ft,

Δr_{jet} = the reduction of the jet radius caused by mass loss.

The number of drops of radius r_m formed is approximated as the number of drops required to fill the outer edge of the oxidizer jet.

$$2\pi r_{jet} = N_{drops} \left(2 r_m \right) \tag{5}$$

where r_{jet} = the radius of the oxidizer core stream in ft,

N_{drops} = the number of drops created,

r_m = the radius of the drop created in ft.

The volume of the drops is subtracted from the jet, and a new liquid jet radius is calculated. The next droplet radius is then calculated using the new jet size. This process continues until the liquid jet disappears.[3]

With all possible drop sizes known, the mass median drop size (r_{mm}) and the standard deviation of drop sizes (σ_g) are computed. These values are used to calculate three representative drop sizes.

$$r_1 = r_{mm} / \sigma_g \tag{6}$$

$$r_2 = r_{mm} \tag{7}$$

$$r_3 = r_{mm} \cdot \sigma_g \tag{8}$$

The two non-median sizes (r_1 and r_3) are each assumed to constitute 16.5% of the total number of drops created, and the median drop size (r_2) to make up the other 67%. This process of drop size calculation is repeated for each injector.[3]

After droplets form they are acted on by drag forces from the gas flow. These forces either accelerate or decelerate the drops, depending on their relative velocities. As the drops move downstream, they continue to vaporize. That vapor is added to the gas flow uniformly by distributing $^1/_8$ of the vapor mass to grid cells at 45° increments around the droplet. The droplets are tracked until they completely vaporize, the flow reaches the throat, or a droplet impinges on the chamber wall. If impingement occurs the drop is assumed to instantaneously vaporize, and all of the drop's mass is added to the gas flow in the nearest grid cell.

PLC uses the Priem-Hiedmann Generalized Length Correlation[6] to vaporize the oxidizer droplets. The correlation is based on the premise that propellant vaporization is the process that controls the combustion rate in a rocket. The correlation attempts to show how various combustion chamber parameters (chamber length, nozzle convergence length, contraction ratio, nozzle shape, injection velocity, chamber pressure, drop size, and initial propellant temperature) effect propellant vaporization. The generalized length parameter is defined as[6]

$$l_{gen} = \left(\frac{l_c}{cr^{0.44}} + \frac{0.83 l_n}{cr^{0.22} S^{0.33}}\right)\left(\frac{P/300}{\left(1 - T_{l\rho,R}\right)^{0.4}\left(\frac{r_m}{0.003}\right)^{1.45}\left(\frac{v_o}{1200}\right)^{0.75}\left(\frac{\lambda}{140}\right)^{0.8}\left(\frac{M_a}{100}\right)^{0.35}}\right) \quad (9)$$

where l_{gen} = the generalized length in inches,

l_c = the cylindrical chamber length in inches,

l_n = the nozzle convergence length in inches,

cr = the nozzle contraction ratio,

S = the nozzle shape factor

(nozzle volume/cylindrical chamber volume),

P = the total chamber pressure in psi,

$T_{l,o,r}$ = the reduced initial propellant temperature

(initial propellant temperature/critical propellant temperature),

r_m = the drop radius in inches,

v_o = the initial drop velocity in inches/sec,

λ = the latent heat of vaporization of the oxidizer in BTU/lb,

M_a = the molecular weight of the oxidizer in lb_m/lb_{mole}.

In PLC this generalized length correlation is tabulated with experimental mass vaporization data to estimate vaporization percentages. PLC calculates the generalized length for each drop size. This value is used with the tabulated vaporization data to estimate the amount of mass that will be vaporized from a droplet. This process is repeated at each axial location until the droplets disappear.

The drops and vapor from each injector are assumed to move downstream in circular streamtubes centered on the injector axis. These streamtubes expand like a cone from the injector, and can overlap one another, until the sum of all streamtube circular areas equals or exceeds the chamber cross-sectional area at that axial distance from the injector plate. PLC then assumes that the cross-section is filled with vapor and begins to assign vapor mass to the grid cells.

The vapor mass distribution routine assumes that flow from the outermost ring of injectors will form an annulus against the chamber wall. This annulus has the same area as the sum of the streamtube areas in that injector ring. The annulus is then divided into segments. Each segment has the same area as its corresponding streamtube with the first segment beginning at 0° and replacing the streamtube whose angular position is closest to 0°. This process is repeated for every ring of injectors, with each annulus abutting the next outermost ring. With these new areas defined, "apparent" injector locations at the center of the sections are assigned (See Figure 3). The new injector and streamtube locations are used to distribute mass to the grid based on the degree to which the grid cells overlap the apparent streamtube areas. After the vapor is distributed, PLC smooths the mass distribution in the chamber cross-section by averaging the mass in the cells. This smoothed mass flow distribution in turn forces a uniform pressure profile. The mass distribution is resmoothed at every axial step in the cylindrical portion of the chamber.

Efficiencies are calculated at the nozzle throat. An oxygen vaporization efficiency, η_{vap} is calculated from

$$\eta_{vap} = \frac{m_{vap_{ox}}}{m_{tot_{ox}}} \tag{10}$$

where m_{vapox} = total oxidizer vapor mass flow

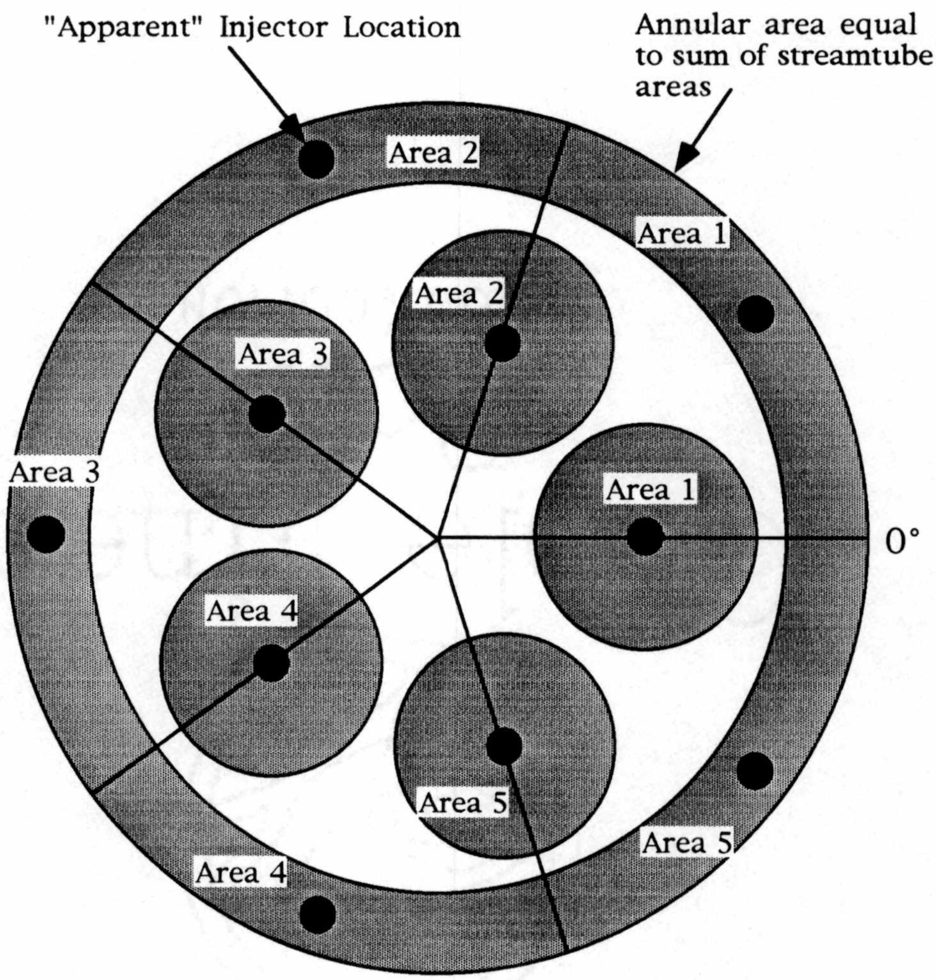

Figure 3. Vapor mass distribution.

m_{totox} = total oxidizer mass flow.

The value of η_{vap} is used to determine if the chamber is long enough to allow complete vaporization. An energy release, or C* efficiency is also calculated.

$$\eta_{ere} = \frac{C^*_{exp}}{C^*_{theo}} \tag{11}$$

where C^*_{exp} = the characteristic exhaust velocity based on measured combustor characteristics in a real experimental setup, or, in the PLC program, is a mass-averaged local C* over the throat cross-section,

$$C^*_{exp} = \sum_{i=1}^{nseg} \sum_{j=1}^{nslice} \frac{C^*_{ij} \cdot m_{ij}}{m_{tot}} \tag{12}$$

where C^*_{ij} = the characteristic exhaust velocity for cell i,j in ft/sec,

m_{ij} = the mass flow in cell i,j in lb_m/sec,

m_{tot} = the total mass flow in the chamber in ft/sec.

C^*_{theo} = the characteristic exhaust velocity that would be attained if there was complete and uniform vaporization of the fuel and oxidizer at the overall mixture ratio.

PLC obtains these values of C* with its gas property interpolation routine. The final efficiency calculated by PLC is defined as a “mixing efficiency,” η_{mix}, where

$$\eta_{mix} = \frac{\eta_{ere}}{\eta_{vap}} \tag{13}$$

The value of η_{mix} will be approximately equal to η_{ere} for cases with complete or almost complete oxidizer vaporization.

Modifications to PLC Code

Based on analysis of the modeling done by PLC, the author decided that several problem areas in PLC's method for distribution of vapor mass to cells and droplet movement from cell to cell must be addressed. The procedure to force vapor mass into annular regions is a poor modelling method. It completely alters the input spray patterns and results in different injector patterns displaying the same downstream flow patterns. This procedure was altered by removing that section of the program which distributes the mass, and replacing it with a new subroutine. The new routine also distributes vapor mass to grid cells, but does so without altering the location of the injectors or the streamtubes.

In the new method for distributing vapor mass, the vapor mass is added to those grid cells touched by a streamtube. The the appropriate grid cells are found by first computing the distance between the center of the streamtube and the grid cell (See Figure 4). Then the radius of a circle with an area equal to that of the grid cell under consideration is calculated, and that radius is added to the radius of the streamtube. If the distance between centers is less than or equal to the sum of the radii, then the streamtube is

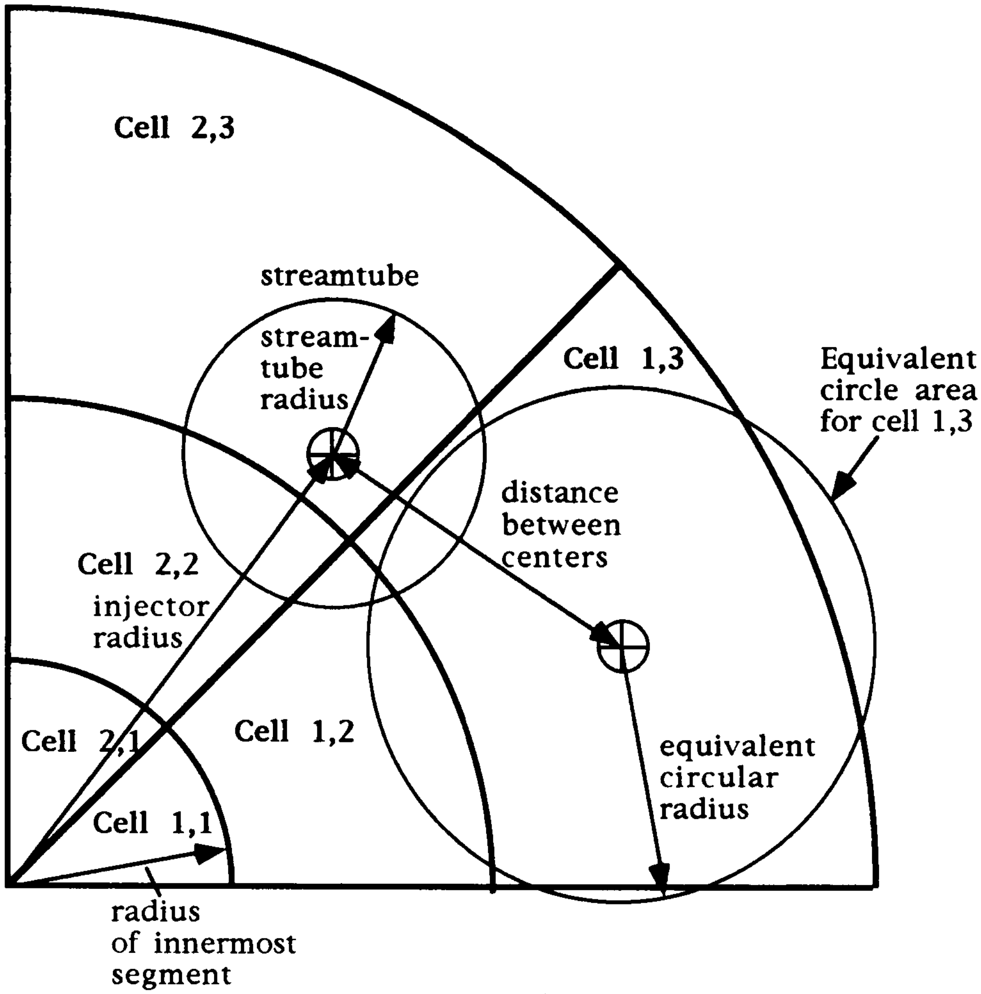

In this figure, the streamtube shown overlaps cells: 1,2; 1,3; 2,2; 2,3

Figure 4. Determination of streamtube overlap.

assumed to touch the cell. A numerical factor, α, can be used to scale the sum of radii to allow for variations in the degree of approximation of which cells are overlapped by a streamtube. In the present study α=1.35 was used. No optimization study for α was carried out, however. If a grid cell is found to be touched by a streamtube, vapor is added to that cell. If the streamtube radius is greater than the distance between centers, all of the mass from that streamtube is added to that cell. If the distance between centers is greater than the streamtube radius, half of the vapor mass is added to the cell. This procedure is repeated for all injectors until all of the grid cells touched have been found.

At this point the total mass in the cross-section far exceeds the actual mass in the flow. To correct this defect, all of the mass in all of the cells is summed and the percentage of this total mass that is in each cell is calculated. The same percentage of the correct total fuel and oxidizer mass flows is then assigned to the grid cells. This process for flow distribution is not exact, but it offers a simple approximation that is, in the author's opinion, considerably more realistic than the original method.

PLC's original procedure of forcing a uniform pressure distribution by averaging the mass flow in the cells is extremely damaging to the flow profile. The process wipes out flow irregularities and makes impossible any analysis of performance fluctuations caused by injector pattern variation. To alleviate this problem, the section of PLC responsible for the mass averaging was eliminated.

The efficiencies computed by PLC are valuable and useful to characterize combustor or throat chamber performance. However the energy release or C*-efficiency could be calculated in different ways. Therefore, in the present study additional ways of computing C*-efficiency were explored. In the course of flow development, PLC uses the constant input chamber pressure throughout the flow. To check the validity of this assumption, two different methods of defining or calculating P_c were investigated. An effective chamber pressure and average chamber pressure were calculated, both based on mass flow passing through the throat of the nozzle. These two pressures offer the extremes of possible chamber pressure in the combustor. The effective chamber pressure, P_{ceff}, is calculated as the area-weighted average of the individual cell stagnation pressures that depend only on the properties and mass flow in each cell. On the other hand, the average chamber pressure, P_{cavg}, is based on the assumption that each cell has the same stagnation pressure, regardless of the mass in that cell.

In the calculation procedure for the effective chamber pressure, the pressure in each cell is determined based on mass flow, mixture ratio and gas properties in that cell, and the effective chamber pressure (P_{ceff}) was calculated as an area-weighted average of individual cell pressures, as follows.

$$P_{c_{eff}} = \sum_{i=1}^{nseg} \sum_{j=1}^{nslice} \frac{P_{c_{ij}} \cdot A_{ij}}{A_{cs}} \tag{14}$$

where P_{cij} = the stagnation pressure in cell i,j in psi,

$$P_{c_{ij}} = \frac{m_{vap_{ij}}}{A_{ij}} \sqrt{\frac{RT_{ij}}{\gamma_{ij} g_c M_{ij}}} \left(\frac{\gamma_{ij} + 1}{2} \right)^{\frac{\gamma_{ij}+1}{2(\gamma_{ij}-1)}} \tag{15}$$

where m_{vapij} = vapor mass in cell i,j in lb_m/sec,

T_{ij} = the total temperature in cell i,j in °R,

γ_{ij} = ratio of specific heats in cell i,j,

M_{ij} = the molecular weight of the gas in cell i,j in lb_m/lb_{mole},

$g_c = 32.2 \text{ (ft lb}_m)/(\text{lb}_f \text{ sec}^2)$,

$R = 1545.3 \text{ (ft lb}_f)/(\text{lb}_{mole}{}^\circ\text{R})$ (the universal gas constant),

A_{ij} = the area of cell i,j in $inches^2$,

A_{cs} = the area of the cross-section in $inches^2$.

This is an iterative calculation, because the gas properties in the cells are based on pressure, so the pressure calculation must be repeated until P_{ceff} converges to a constant value. Note that the properties determined in this way represent stagnation values for each cell.

The average chamber pressure was calculated by first finding the gas properties in each cell, using the input or design value of P_c. These properties and the total vapor mass flow were used to determine the average chamber stagnation pressure as follows:

$$P_{c_{avg}} = \frac{m_{vaptot}}{\sum_{i=1}^{nslice} \sum_{j=1}^{nseg} \sqrt{\frac{\gamma_{ij} M_{ij} g_c}{R T_{ij}}} \left(\frac{\gamma_{ij} + 1}{2} \right)^{\frac{-(\gamma_{ij}+1)}{2(\gamma_{ij}-1)}} A^{*}_{ij}} \tag{16}$$

where m_{vaptot} = the total vapor mass flow in lb_m/sec,

γ_{ij} = ratio of specific heats in cell i,j,

M_{ij} = the molecular weight of the gas in cell i,j in lb_m/lb_{mole},

g_c = 32.2 (ft lb_m)/(lb_f sec^2),

R = 1545.3 (ft lb_f)/(lb_{mole}°R) (the universal gas constant),

T_{ij} = the total temperature in cell i,j in °R,

A^*_{ij} = the area of cell i,j at the throat in ft^2.

The calculation of P_{cavg} is also an iterative process much like that for P_{ceff}, because stagnation gas properties in the various cells depend on the chamber pressure, P_{cavg}, which is a result of the calculation.

As an ideal reference pressure, the ideal stagnation pressure, P_{ceq}, an equilibrium chamber pressure (P_{ceq}) is calculated based on the assumption that all of the input fuel and oxidizer are completely reacted, and form an equilibrium gas at the overall mixture ratio. Thus,

$$P_{c_{eq}} = \frac{m_{tot}}{A_{cs}} \sqrt{\frac{RT}{\gamma g_c M}} \left(\frac{\gamma + 1}{2} \right)^{\frac{\gamma+1}{2(\gamma-1)}} \quad (17)$$

where m_{tot} = the total mass flow,

A_{cs} = the cross-sectional area of the throat,

R = the universal gas constant,

T = the gas temperature,

γ = the ratio of specific heats,

M = the molecular weight of the gas.

For this computation, all gas properties depend on the overall vapor mixture ratio and chamber pressure and therefore, the solution for P_{ceq} is also an iterative one.

With these "chamber" pressures defined, it is possible to also define two additional efficiencies, and a pressure non-uniformity parameter. The additional efficiencies and the stagnation pressure non-uniformity parameter that were calculated were defined as follows. A combustion efficiency, η_c, was defined as

$$\eta_c = \frac{C^*\left(P_{c_{eff}}\right)}{C^*\left(P_{c_{orig}}\right)} \tag{18}$$

where

$$C^*(P_{c_{eff}}) = \frac{P_{c_{eff}} \cdot Acs}{\dot{m}_{tot}} \tag{19}$$

and $C^*(P_{corig})$ comes from the interpolation tables; it is the C^* that corresponds to the overall mixture ratio and input chamber pressure. The stagnation pressure non-uniformity parameter was defined, and calculated as follows.

$$\eta_P = \frac{P_{ij\max} - P_{ij\min}}{P_{ceff}} \tag{20}$$

where P_{ijmax} = the maximum cell stagnation pressure,

P_{ijmax} = the minimum cell stagnation pressure.

η_P gives a measure of the non-uniformity of the distribution of stagnation pressure over the chamber cross-section. The third efficiency calculated by PLC is the ratio of average chamber stagnation pressure to equilibrium chamber stagnation pressure, η_{c^*}, where

$$\eta_{c^*} = \frac{P_{c_{avg}}}{P_{c_{eq}}} \tag{21}$$

This efficiency is most closely comparable to actual rocket motor C* efficiencies used in rocket motor performance evaluations. Note that η_{c*} corresponds , in principle, if not in the way its calculated, to η_{ere} defined in the original PLC code. Also note that in all cases, it is assumed that the static pressure is constant across the chamber at any axial station, although it can and will vary axially, i.e., from injector plate to nozzle throat.

CHAPTER THREE

INJECTOR PATTERN ANALYSIS

After modification, PLC was used to gain a qualitative understanding of how variations of injector layouts can effect combustion efficiency. Different injector patterns were analyzed with PLC and the outputs were compared. Patterns were varied in both the numbers and placement of coaxial injectors. The Sample input file included with the PLC program as a reference case was taken as the base pattern (See Figure 5). The propellant properties, nominal chamber pressure, chamber geometry and overall mass flow of this reference case were chosen as the given or fixed conditions for all cases studied. Nine different injector pattern configurations were studied in the thesis research. Drawings of the selected injector configurations are included in Appendix A, and some layout parameters are shown in Table 1.

Geometric parameters were developed to characterize injector layout (See Figure 6). The parameters include a space factor (Si) to describe the arc length between injectors on a ring,

$$S_i = \frac{2\pi r_i}{N_i} \tag{22}$$

where r_i = radius of the ith ring of injectors in inches,

N_i = the number of injectors on the ith ring,

a pitch factor (Pij) to characterize the spacing between rings,

$$P_{ij} = \frac{\Delta S_{ij}}{\Delta r_{ij}} \tag{23}$$

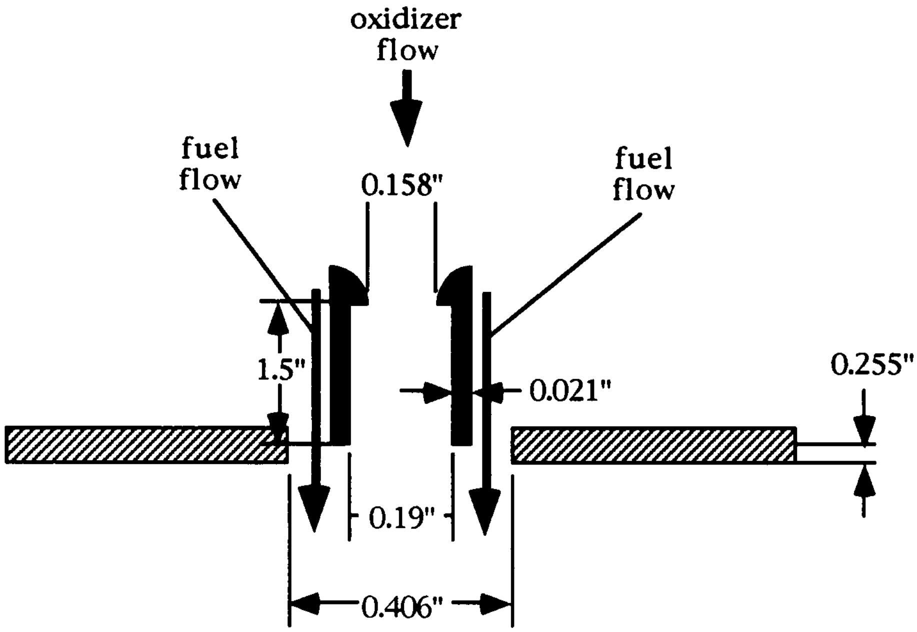

(a) Injector dimensions

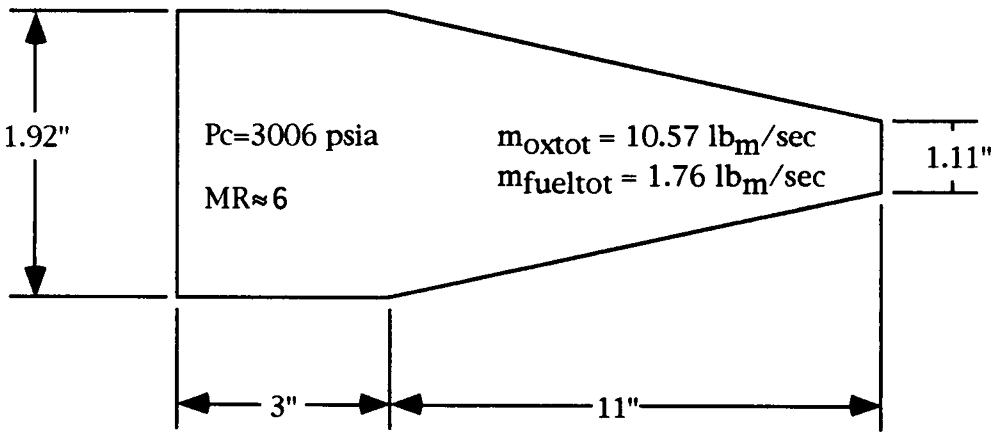

(b) Chamber dimensions

Figure 5. Sample Case Input Parameters.

Note: Figures are not drawn to scale.

Table 1. Injector layout configurations.

Pattern Number	Number of Injectors	Number of Rings	Injector Sizing Constant C_{inj}	Fuel Mass Flow per Injector	Oxidizer Mass Flow per Injector
Sample	7	1	1.0	$0.4343 + 0.04353\sin\theta$	1.3145
1:7a	7	1	1.0	$0.4343 + 0.04353\sin\theta$	1.3145
1:7b	7	1	1.0	0.4353	1.3145
1:7c	7	1	0.4	0.4353	1.3145
2:4,8	13	2	0.4	0.2343	0.7078
3:4a	13	3	0.4	0.2343	0.7078
3:4b	13	3	0.4	0.2343	0.7078
3:4c	13	3	0.4	0.2343	0.7078
3:6,12,12	31	3	0.4	0.0983	0.2968

Note: The pattern number is composed of two types of numbers. The first number denotes the number of concentric rings, and the second set of numbers denotes the number of injectors on each ring. Letters after a pattern number differentiate between pattern with the same arrangement of rings.
i.e. the number 2:4,8 mean two rings of injectors, the first having four injectors and the second having eight injectors. If only one number is given for number of injectors per ring, each ring has an equal number of elements.

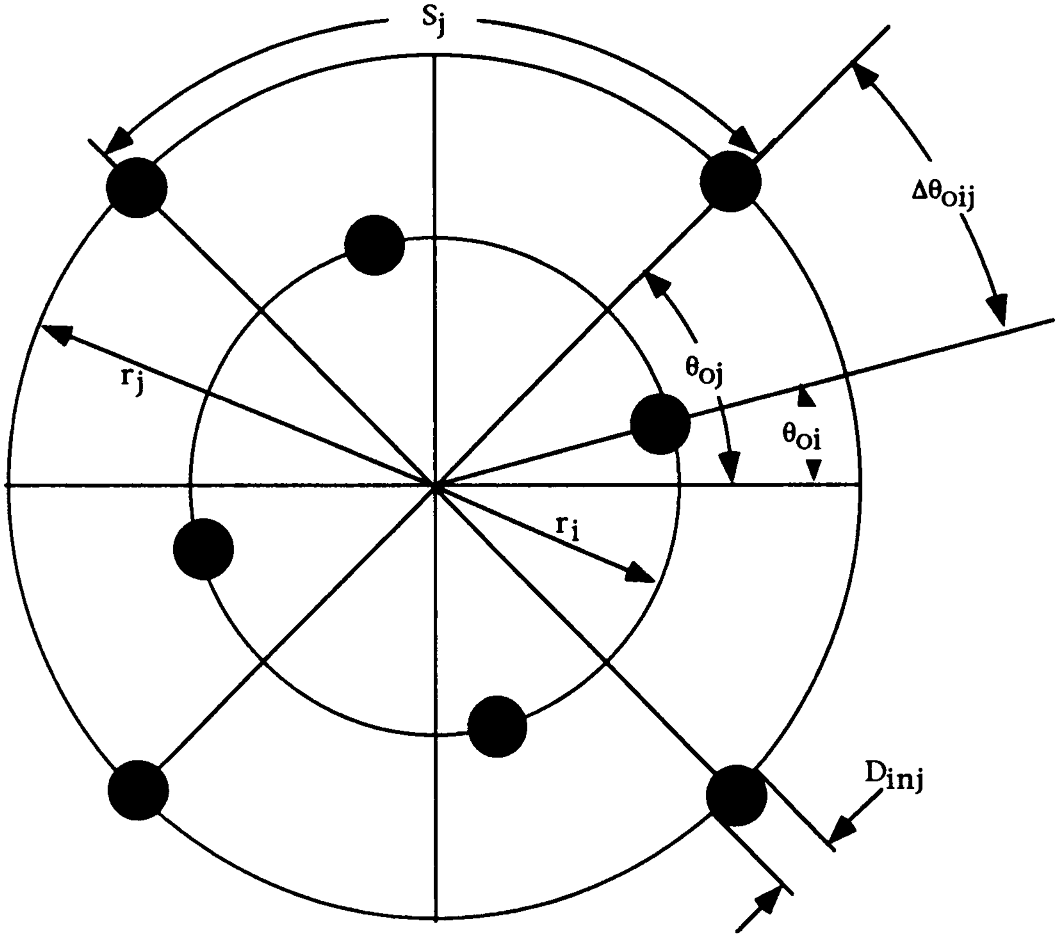

Figure 6. Geometric parameters

where $\Delta S_{ij} = S_i - S_j$,

$\Delta r_{ij} = r_i - r_j$,

and an angle factor ($\Delta\theta_{Oij}$) to represent the angular displacement between the injectors on adjacent rings.

$$\Delta \theta_{oij} = \left| \theta_{oi} - \theta_{oj} \right| \qquad (24)$$

where θoi = the angular location of the first injector on the ith ring,

θoj = the angular location of the first injector on the jth ring.

The overall injector plate porosity (ε) describing the percentage of the total plate area covered by the injectors,

$$\varepsilon = \frac{A_I}{A_P} \qquad (25)$$

where A_I = total flow area of all injector elements in ft^2,

A_P = total injector plate area in ft^2,

and a local plate porosity (ε_{ij}) characterizing the porosity between two rings of injectors are also used.

$$\varepsilon_{ij} = \frac{A_{E_{ij}}}{A_{ij}} = \frac{(N_i + N_j) \cdot D_{inj}}{8 \cdot \left(r_i^2 - r_j^2\right)} \qquad (26)$$

where A_{Eij} = area of injectors between rings i and j in ft^2,

A_{ij} = area of plate between rings i and j in ft^2,

N_i = the number of injectors on ring i,

N_j = the number of injectors on ring j,

D_{inj} = the diameter of an injector in ft,

r_i = the radius of ring i, in ft,

r_j = the radius of ring j, in ft,

These numerically based geometric parameters can be used as a rational method of cataloging, scaling and comparing different injector distribution patterns. However, in the present study, these geometric parameters were not utilized or analyzed. Rather, this thesis attempts to define some numerical parameters for characterizing injector patterns, and lists some typical values for injector geometries studied. Additional study and research is required in order to determine the value of such numerical characterizations of injector patterns. A literature search on this topic was conducted but no useful information had been found at the time of writing. The sets of parameters calculated for each of the injector patterns studied herein are shown in Table 2.

Before the study of injector patterns was made, an analysis was conducted of PLC's sensitivity to geometric variations between injector and chamber geometry. Chamber and injector geometries were varied to determine their effect on the PLC output (See Table 3). This study showed that the program results were very sensitive to injector geometry, indicating that the submodels may have a relatively narrow range of applicability. For example, doubling the injector diameter resulted in unreasonably large calculated gas velocities. The study also showed unfavorable effects from increasing the mass flow without altering the input chamber pressure. Initial error would be expected because changing the mass flow without changing the pressure introduces mass flow conservation errors. The study showed that changes in mass flow, and

Table 2. Injector Pattern Geometric Parameters.

Pattern Designation	Number of Rings N_R	Number of Injectors per Row N_i	Spacing Factor (in) S_i	Pitch Factor P_{ij}	Angle Factor (degrees) $\Delta\theta_{Oij}$	Total Plate Porosity ε	Local Plate Porosity ε_{ij}
1:7a (Sample)	1	N_1=7	S_1=0.61	N/A	N/A	0.3127	N/A
1:7b	1	N_1=7	S_1=0.61	N/A	N/A	0.3127	N/A
1:7c	1	N_1=7	S_1=0.61	N/A	N/A	0.067	N/A
3:6,12,12	4	N_1=1 N_2=6 N_3=12 N_4=12	S_1=0 S_2=0.251 S_3=0.251 S_4=0.251	P_{21}=1.05 P_{32}=0 P_{43}=0.524	$\Delta\theta_{O21}$=0 $\Delta\theta_{O32}$=15 $\Delta\theta_{O43}$=15	0.125	ε_{21}=0.226 ε_{32}=0.194 ε_{43}=0.155

Table 2. (cont.)

Pattern Designation	Number of Rows N_R	Number of Injectors per Row N_i	Spacing Factor (in) S_i	Pitch Factor P_{ij}	Angle Factor (degrees) $\Delta\theta_{oij}$	Total Plate Porosity ε	Local Plate Porosity ε_{ij}
2:4,8	3	$N_1=1$ $N_2=4$ $N_3=8$	$S_1=0$ $S_2=0.503$ $S_3=0.503$	$P_{21}=1.57$ $P_{32}=0$	$\Delta\theta_{O21}=0$ $\Delta\theta_{O32}=0$	0.125	$\varepsilon_{21}=0.217$ $\varepsilon_{32}=0.173$
3:4a	4	$N_1=1$ $N_2=4$ $N_3=4$ $N_4=4$	$S_1=0$ $S_2=0.377$ $S_3=0.754$ $S_4=1.13$	$P_{21}=1.57$ $P_{32}=1.57$ $P_{43}=1.57$	$\Delta\theta_{O21}=0$ $\Delta\theta_{O32}=45$ $\Delta\theta_{O43}=-45$	0.125	$\varepsilon_{21}=0.385$ $\varepsilon_{32}=0.205$ $\varepsilon_{43}=0.123$
3:4b	4	$N_1=1$ $N_2=4$ $N_3=4$ $N_4=4$	$S_1=0$ $S_2=0.377$ $S_3=0.754$ $S_4=1.13$	$P_{21}=1.57$ $P_{32}=1.57$ $P_{43}=1.57$	$\Delta\theta_{O21}=0$ $\Delta\theta_{O32}=30$ $\Delta\theta_{O43}=30$	0.125	$\varepsilon_{21}=0.385$ $\varepsilon_{32}=0.205$ $\varepsilon_{43}=0.123$
3:4c	4	$N_1=1$ $N_2=4$ $N_3=4$ $N_4=4$	$S_1=0$ $S_2=0.377$ $S_3=0.754$ $S_4=1.13$	$P_{21}=1.57$ $P_{32}=1.57$ $P_{43}=1.57$	$\Delta\theta_{O21}=0$ $\Delta\theta_{O32}=0$ $\Delta\theta_{O43}=0$	0.125	$\varepsilon_{21}=0.385$ $\varepsilon_{32}=0.205$ $\varepsilon_{43}=0.123$

Table 3. Results of PLC sensitivity study.

Variation from Sample Input File	Results
Double chamber length and radius	reasonble results
Double chamber radius and injector dimensions	unreasonable results
Double chamber radius, injector dimensions, and mass flow	unreasonable results
Double chamber length, radius and injector dimensions	unreasonable results
Double chamber length and radius used two rows of injectors: 4 elements at r=0.6403" 8 elements at r=1.281"	reasonable results

combustion chamber and injector geometry could not be arbitrary. The parameters can be varied only over limited ranges which apparently correspond to the limits of the physical submodels. Rather than pursue a study to map out all the values of the geometric and injector parameters that will yield reasonable program output, a much more limited study was attempted, a study of injector distribution patterns on combustion efficiency. Changes in injector conditions such as injector diameters and mass flows were done in such a way that the propellant injection velocities were reasonably close to the values in the sample or reference case.

The Sample case chamber dimensions were used for all injector patterns. The propellant properties and total mass flows were also held constant. The Sample case geometry and properties are shown in Figure 5. Injector size varied for the different cases because of the physical constraints of the injector plate and the element configuration. All injector dimensions were scaled from the sample case in order to maintain the relative size of the elements and the relative velocity difference between hydrogen gas flow and liquid oxygen jet core flow. This scaling factor was

$$Sc = \frac{D_{inj_{pattern}}}{D_{inj_{sample}}} = \sqrt{C_{inj} \frac{N_{inj_{sample}}}{N_{inj_{pattern}}}} \tag{27}$$

where Sc = the scaling factor,

$D_{inj\ pattern}$ = outer diameter of injector of current pattern,

$D_{inj\ sample}$ = outer diameter of injector of sample pattern,

C_{inj} = propellant injection velocity ratio, sample case velocity divided by current pattern velocity,

$N_{inj\ sample}$ = number of injectors in the sample pattern,

$N_{inj\ pattern}$ = number of injectors in the current pattern.

If C_{inj} equals one, injection velocities match for different sizes of injectors. A value of one for C_{inj}, however, proved to be too large for most configurations because the injectors would be so large that they would overlap. Therefore, most cases studied used a value of C_{inj} = 0.4 (See Table 1). This means that those patterns with more than seven elements had injection velocities about 2.5 times those for the seven element configurations.

Seven, thirteen, and thirty-one element patterns were studied. Two different seven element patterns were chosen to compare to the seven element sample case. Thirteen and thirty-one injector patterns were chosen to investigate a wide range of injector configurations. There were four thirteen element patterns studied. They were used to analyze the effect of injector placement on the combustion performance. Element injector locations, for seven and for thirty-one elements, were not varied because of the limited arrangement options for the seven element layout, and physical space constraints for the thirty-one element layout. The three seven element patterns provide a comparison of the effects of injector size and mass flow distribution.

For all patterns a variable mass distribution scaling factor, α, was used. This factor was based on the ratio of the injector ring to the radius of the innermost grid segment (See Figure 4).

$$\alpha = \begin{cases} 1.0 & \text{if rinj/rsegl} \leq 1.0 \\ 1.35 & \text{if rinj/rsegl} > 1.0 \end{cases} \tag{28}$$

The variable values of α were determined by trial and error. The streamtubes were drawn on a diagram of the grid structure to determine which grid cells were actually touched by the streamtubes. The scaling factor, α, was varied in PLC until the grid cell predicted to be overlapped matched the actual overlapped grid cells.

CHAPTER FOUR

RESULTS

From the injector pattern analysis conducted, two main sets of results are presented: chamber pressures and combustor efficiencies, and mixture ratio distributions. The efficiencies calculated for each configuration are shown in Table 4. Plots of the mixture ratio profiles are included in Appendix B. All output denoted as "sample" was produced by the unmodified PLC program analyzing the sample input file. The input file for "sample" and case 1:7a were identical however.

Efficiencies and mixture ratios are not the only output provided by PLC. A typical output file can be seen in Figure 7. This is not the only output file provided by PLC, but it is probably the most useful. Additional output includes: cell mixture ratios at all axial locations, cell mass flows at each axial location, a record of droplet movement, droplet vaporization at each axial location, cells to which drop vapor is distributed, gas velocities at each axial location, and total amount of fuel and oxidizer vaporized. In addition to the mixture ratio plots in Appendix B, pressure, molecular weight, gas temperature, fuel vapor mass flows, oxidizer vapor mass flows, C*, and density profiles could also be generated.

The oxidizer vaporization efficiency is ≈100% for all patterns studied (See Table 4). This value should be approximately constant for all the cases studied because the percentage of mass vaporized depends mainly on the length of the chamber and not on injector layout. Also, the combustion chamber utilized in the present study is fairly ling. Therefore, the oxidizer

Table 4. Calculated efficiencies for various injector configurations.

Pattern Number	Oxidizer Vaporization Eff. η_{vap}	Energy Release Eff. η_{ere}	Mixing Eff. η_{mix}	C* Eff. η_c	Pressure Eff. η_p	Average Pressure Eff. η_{c^*}
Sample	100.0	88.199	88.199	N/A	N/A	N/A
1:7a	99.982	99.617	99.635	99.711	44.725	95.023
1:7b	99.983	99.486	99.503	99.597	45.360	96.375
1:7c	99.986	99.918	99.932	100.033	37.648	96.691
2:4,8	99.998	98.721	98.723	98.727	155.850	100.474
3:4a	99.997	98.449	98.452	98.454	191.269	100.418
3:4b	99.997	99.072	99.075	99.150	223.629	100.371
3:4c	99.997	99.128	99.131	99.291	220.437	100.373
3:6,12,12	99.998	99.354	99.356	99.366	121.530	99.982

SAMPLE INPUT FILE ONE
ROW TYPE INPUT FOR SINGLE ROW SEVEN ELEMENT SHEAR COAX

1.763 LB/SEC OF FUEL VAPORIZED OUT OF 1.763 LB/SEC TOTAL
10.577 LB/SEC OF OX VAPORIZED OUT OF 10.579 LB/SEC TOTAL

OX VAPORIZATION EFFICIENCY= 99.982%
MIXING EFFICIENCY=101.247%
ENERGY RELEASE EFFICIENCY=101.228%

PC1 (starting value)= 3006.000000000000

THETA,	RGRID,	PCMASS,	XMASS,	HMASS,	RATM
0.00,	0.00,	3022.055,	0.937,	0.131,	7.133
0.00,	0.03,	3893.901,	1.122,	0.195,	5.739
60.00,	0.00,	2606.183,	0.736,	0.137,	5.369
60.00,	0.03,	2653.323,	0.753,	0.138,	5.442
120.00,	0.00,	2529.850,	0.718,	0.132,	5.442
120.00,	0.03,	2614.576,	0.752,	0.132,	5.701
180.00,	0.00,	3147.744,	0.869,	0.175,	4.957
180.00,	0.03,	2534.313,	0.745,	0.122,	6.129
240.00,	0.00,	3111.860,	0.865,	0.170,	5.091
240.00,	0.03,	3199.260,	0.900,	0.170,	5.298
300.00,	0.00,	3644.310,	1.064,	0.177,	6.017
300.00,	0.03,	3735.872,	1.106,	0.177,	6.252
360.00,	0.00,	3022.055,	0.937,	0.131,	7.133
360.00,	0.03,	3893.901,	1.122,	0.195,	5.739

PCEFF= 3057.770842105850
PCavg= 2922.133579278737

T= 6369.252056971279
W= 13.07793328931275
G= 1.154199972877612
RT= 5.691839223217598
A*= 6.7346007478785000E-03

ETAC= 0.9986104809395978
ETAP= 0.4460933184166055
ETAC*= 0.9540777915610979

PCEQ= 3062.783354905927

XT= 10.56710028365364
HT= 1.856535272561698
TMASS= 12.42363555621534

Figure 7. Sample output from PLC.

vaporization efficiency should be about the same for all patterns studied in this thesis. The energy release efficiency, η_{ere}, and the mixing efficiency, η_{mix}, range from ~98.4-99.9%. Higher values of η_{ere} correspond to more even C* distributions and therefore more even mass distributions for the cross-section. The same trends can be seen for the C* efficiency, η_c, and for the pressure efficiency, η_p.

Higher η_c values indicate more even mass, and therefore pressure, distributions. This trend is substantiated by η_p. Lower values of η_p indicate a more uniform flow field, and as seen in Table 4, low values of η_p correspond to high values of η_c. η_{c*} ranges from ~95.4-100.12%. Higher values of η_{c*} are found for patterns with thirteen and thirty-one injectors. This indicates that more injector elements better distribute the flow and give an average chamber pressure that more closely matches the equilibrium chamber pressure. This relationship between greater numbers of injectors and improved η_{c*} values is to be expected. A larger number of injectors should provide not only a greater spray coverage than a small number of injectors, but also a more uniform coverage.

The mixture ratio profiles included in Appendix B are, with the exception of Figure 16, a "smoothed" representation of the values provided by PLC. All figures in Appendix B were generated using a plotting program called Spyglass Transform.[7] The "smoothed" plots (See Figures 17-25, Appendix B) were generated by Spyglass Transform by linearly interpolating values between the centers of the cells. Figure 16 shows an unsmoothed Spyglass Transform plot where the mixture ratios predicted by PLC for each cell (the "raw" data) are plotted.

For the "sample" case, the radial variation in mixture ratio was caused by droplet impingement on the chamber walls (See Figure 17, Appendix B). The impingement caused oxidizer drops to vaporize at the wall and increase the mixture ratio in the outer grid cells. The red and yellow areas of extremely high mixture ratios are due to drops from more than one injector impinging in the same grid cell. This problem of apparent non-uniformity could be solved by increasing the number of "slices" used to define the grid from six to twelve (for seven element and one row Nslice=6 and Nseg=2). More grid cells would improve the modeling by allowing more variation within, and greater resolution of, the flow field. The mixture ratio distribution is very uniform circumferentially (except for the area of extra impingement) despite the sinusoidal variation of the input fuel flow (See Table 1) along the circumferential distribution of the injector elements. This apparent resulting uniformity, where none is expected, is caused by the unmodified PLC's method of smoothing the flow field to create a uniform pressure profile.

With the modified PLC code, pattern 1:7a produces a highly unsymmetric mixture ratio distribution (See Figure 18, Appendix B) which is in part due to the circumferential sinusoidal variation of the input fuel flow (See Table 1) to the injectors, and in part due to a lack of grid cells to adequately model the flow. No impingement occurs for this pattern, so the mixture ratios are fairly constant radially except for a small area near the center. The area of high mixture ratios near the center of the cross-section is caused by flow from more than one injector being added to a single grid slice, i.e. spraycone overlap, and the method used in the modified version of

PLC to distribute injector mass flow in the overlapped cells. By increasing the number of slices and segments used to make up the grid, that is, by increasing the numerical resolution, the mixture ratio distributions could be more accurately defined. Increasing the number of slices to twelve and the number of segments to four would bring the grid resolution closer to that of the thirteen and thirty-one element patterns and would provide much improved flow modeling.

The predicted mixture ratio distributions resulting from injector element patterns 1:7b and 1:7c (See Figures 19 and 20, Appendix B) are slightly unsymmetric due to a lack of grid cells to properly model the flow, even though these patterns have the same mass flows issuing from all injector elements. The small variation in the mixture ratios (≈5.5-5.8) for pattern 1:7c should be noted. The distribution is slightly unsymmetric, but since the mixture ratio variation is very low, the pattern's η_p was also very low.

Injector element patterns 2:4,8 and 3:4a produce symmetric mixture ratio distributions (See Figures 21 and 22, Appendix B). The regions of high mixture ratios represent areas of streamtube (or injector spraycone) overlap. The locations of the high mixture ratio concentrations are completely due to the injector layouts (See Figures 11 and 12, Appendix A). Similar results can also be seen for patterns 3:4b and 3:4c. Pattern 3:4b's bent cruciform pattern of high mixture ratio flow (See Figure 23, Appendix B), is a reflection of the similar bent cruciform pattern of the injector layout (See Figure 13, Appendix A) and of streamtube overlap. Pattern 3:4c's straight cruciform high mixture ratio profile (See Figure 24, Appendix B), also reflects its injector layout (See Figure 14, Appendix A) and streamtube overlap. These visual results illustrate precisely why the modifications made to PLC in the present study will be so useful to design and performance engineers. The visualization of the non-uniformity of the flow property distributions caused by injector layout or pattern geometry helps the designer develop an intuitive feel for good (or alternately, bad) patterns.

The concentric rings seen in the mixture ratio profile of pattern 3:6,12,12 (See Figure 25, Appendix B), result from the multiple rings of the injector layout (See Figure 15, Appendix A). The injector rings provide very uniform rings of mass flow. The values vary somewhat radially because of streamtube or spraycone overlap. High mixture ratio areas occur around the middle ring of injectors because streamtubes from both the inner, middle, and outer injector rings touch those middle grid cells.

The areas of low mixture ratio flow near the walls that can be seen in the thirteen and thirty-one element patterns show that PLC may not adequately model vapor movement. It seems unlikely that there would be areas with no oxidizer vapor at all as seen in Figures 23 and 24, Appendix B, because of turbulence effects on distributions, and also radial momentum of oxidizer droplets, in the real rocket chamber. This problem is in part caused by the fact that PLC does not move oxidizer droplets radially to any significant degree and therefore flow tends to concentrate in relatively narrow cone-like regions downstream of the injector, and not spread out. The vapor mass distribution routine, though modified for this thesis, still does not adequately model vapor movement. Radial vapor movement is severely limited, so that the vapor also tends to concentrate in the spraycone configurations, like the droplets. The improvement of the spray modeling for both the vapor phase and the droplet or liquid phase, is an important area for further research and development of the PLC program.

In summary, the results indicate that the best flow distributions and hence the highest efficiencies are given by injector patterns that offer symmetric mixture ratio profiles and the largest areas of even flow coverage, as seen in the thirteen and thirty-one element patterns. This is consistent with both experience and expectation.

CHAPTER FIVE

CONCLUSIONS

The PLC submodel of ROCCID has been modified in the present study to include a technique for a more realistic representation of vapor distribution in a rocket combustion chamber resulting from patterns or layouts of multiple, coaxial fuel injectors. The current version of the program provides output of three dimensional distributions of mixture ratios and gas velocities. Other gas property distributions could be output by PLC with minor modifications. These distributions can be used by designers in assessing injector layout. PLC can also offer estimates of the chamber pressure and C^* efficiency for multi-injector rocket combustion chambers. Thus, the version of PLC developed in the present thesis can help evaluate the effects of different injector patterns on general steady state combustor performance. This would be an extremely useful tool for rocket designer engineers, if a rocket chamber is being designed that only allows for a fixed, small number of injectors.

PLC still needs further improvements, however. The subroutine that distributes vapor mass to grid cells was modified for this thesis, but it only provides a rough estimate of how the vapor should be distributed. A more exact procedure based on overlap geometry that calculates how much of a streamtube actually overlaps a grid cell, and therefore how much mass should be allocated to that cell, should be developed. Changes that account for flow movement from high pressure regions to low pressure regions and that allow more radial droplet movement are needed.

A change in the method of determining the number of grid slices and segments should be made. The number of grid cells should not depend on the number of injectors but on the grid resolution desired by the engineer. PLC should be modified to output three dimensional distributions of other cell gas properties, such as density and temperature, that would be useful analysis tools. In future studies, the chamber length/diameter ratio should be varied parametrically to determine its effects on combustion performance. Also, a comparsion of PLC output and experimental data should be made to validate PLC's predictions.

Without these changes, any output from PLC is suspect, so that at present, PLC should not be used for anything but qualitative analysis. However, even as qualitative tool, it can be extremely useful; it provides visually stimulating results for use in injector layout and pattern analysis in liquid-fueled rocket motors.

LIST OF REFERENCES

LIST OF REFERENCES

[1] Muss, J.A., Nguyen, T.V. and Johnson, C.W., User's Manual for Rocket Combustor Interactive Design(ROCCID) and Analysis Program, Volume I-User's Manual; NASA CR-1087109, May, 1991.

[2] Knuth, W.H. and Crawford, R.A., Oxygen-Rich Combustion Process Applications and Benefits, AIAA-91-2042, June, 1991.

[3] Muss, J.A., Nguyen, T.V. and Johnson, C.W., User's Manual for Rocket Combustor Interactive Design(ROCCID) and Analysis Program, Volume II-Appendixes A-K; NASA CR-187110, May, 1991.

[4] Sutton, George P., Rocket Propulsion Elements: An Introduction to the Engineering of Rockets, 6th edition, John Wiley and Sons, New York, 1992.

[5] Nickerson, G.R., Dang, L.D. and Coats, D.E., Two-Dimensional Kinetic Reference Computer Program (TDK) Engineering and Programming Manual; SEA Report SN63, Final Contract Report for contract NAS8-35931, April 1985.

[6] Priem, Richard J. and Heidmann, Marcus F., Propellant Vaporization as a Design Criterion for Rocket-Engine Combustion Chambers; NASA TR R-67, 1960.

[7] Spyglass Transform v. 2.1; Spyglass Inc., 1992.

APPENDICES

APPENDIX A

INJECTOR PATTERNS

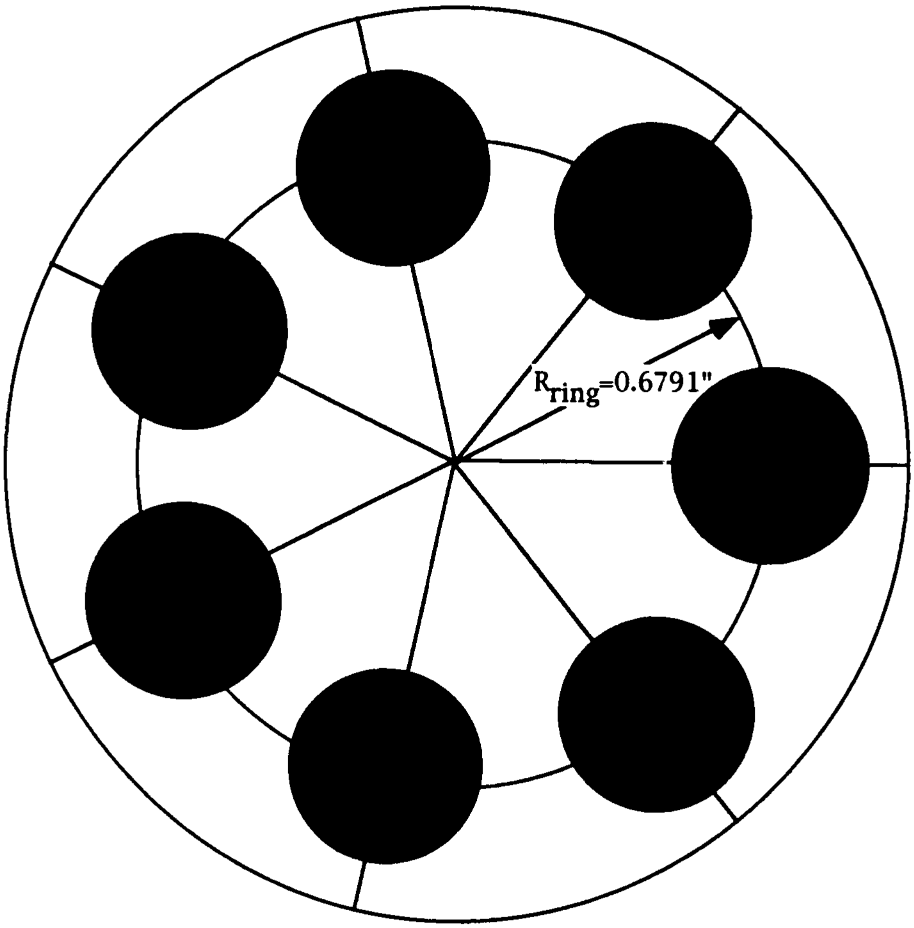

Figure 8. Injector pattern 1:7a

Note: Figure is drawn to 250% scale.

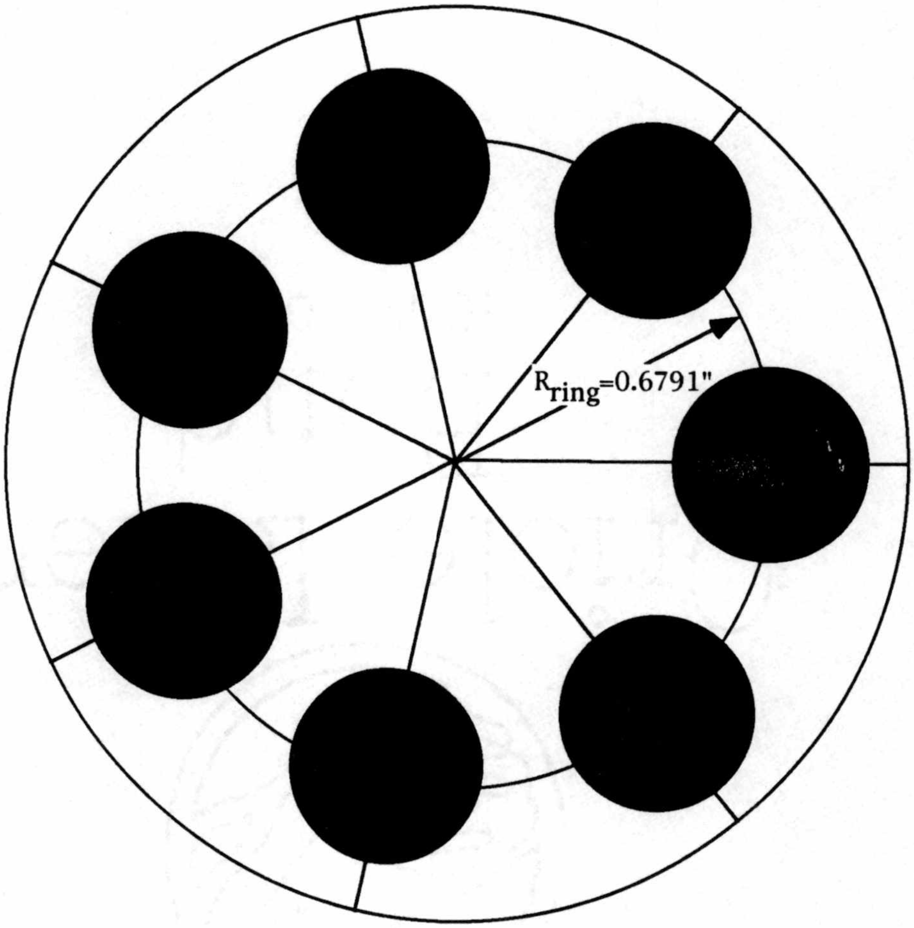

Figure 9. Injector pattern 1:7b.

Note: Figure is drawn to 250% scale.

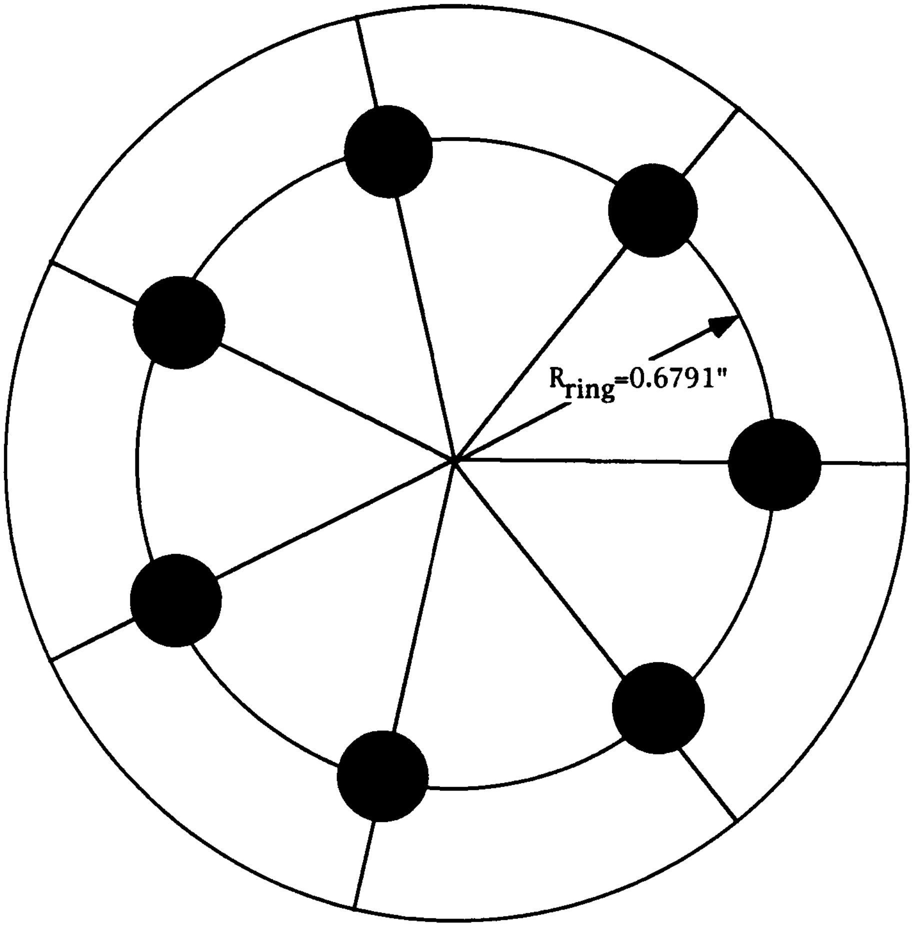

Figure 10. Injector pattern 1:7c

Note: Figure is drawn to 250% scale.

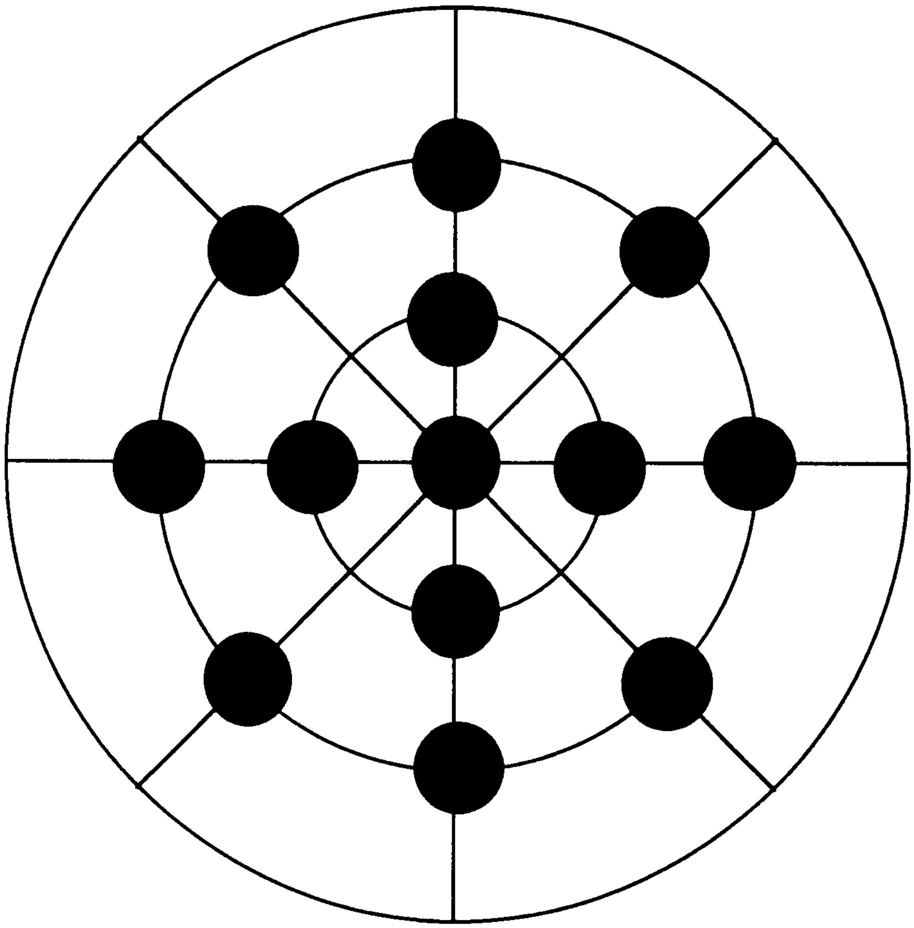

Figure 11. Injector pattern 2:4,8

Note: Figure is drawn to 250% scale.

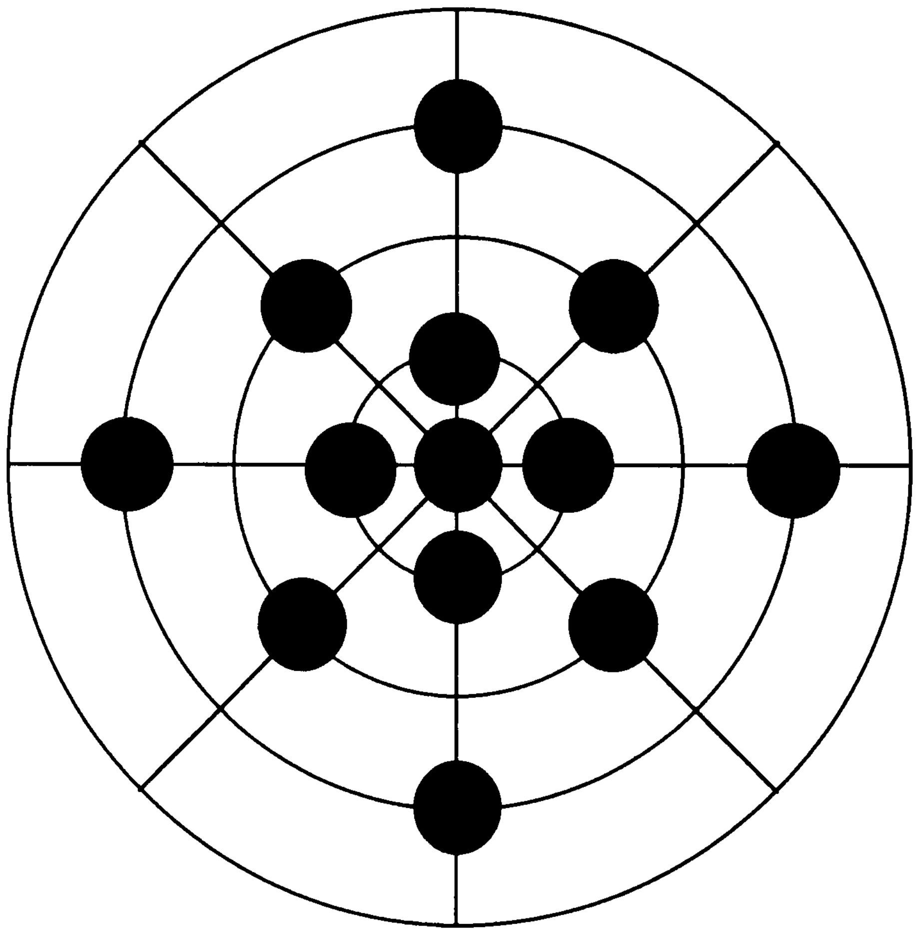

Figure 12. Injector pattern 3:4a

Note: Figure is drawn to 250% scale.

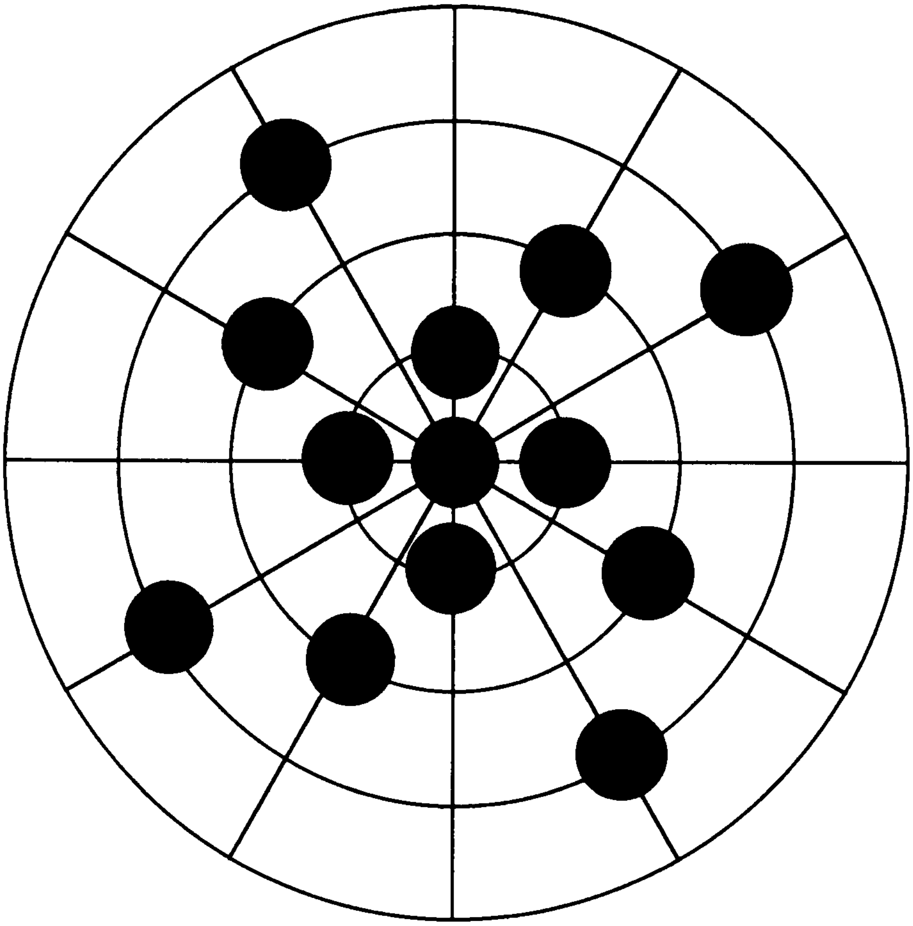

Figure 13. Injector pattern 3:4b

Note: Figure is drawn to 250% scale.

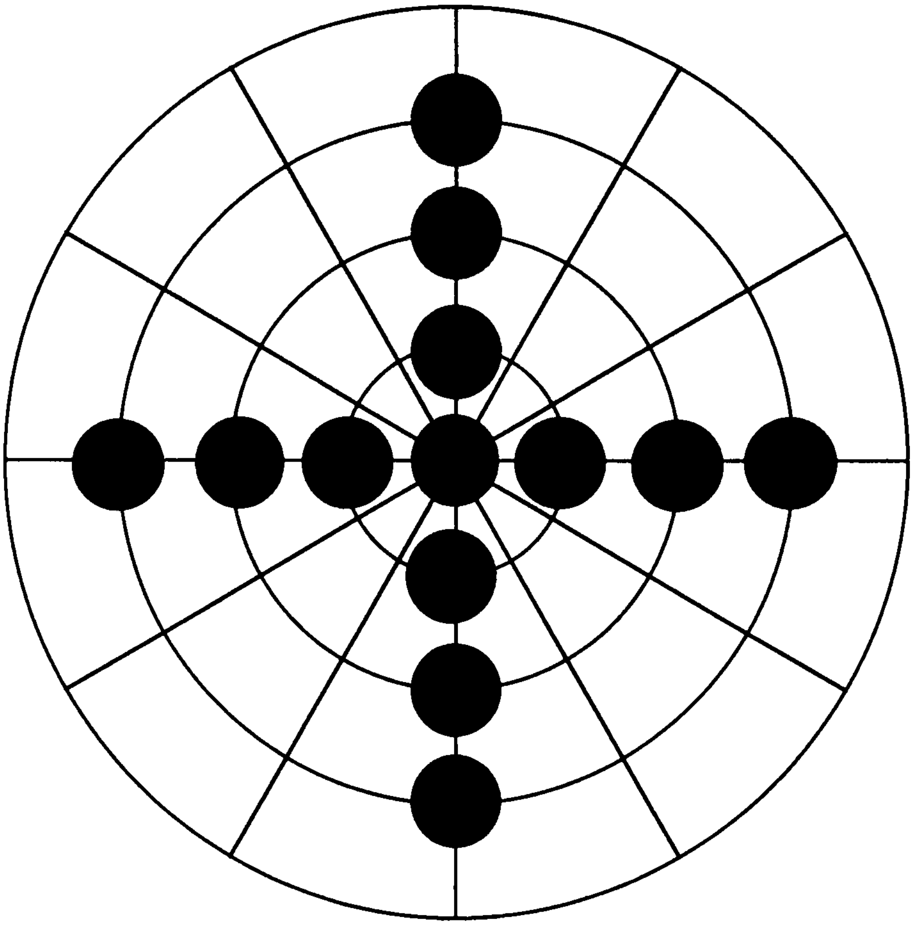

Figure 14. Injector pattern 3:4c

Note: Figure is drawn to 250% scale.

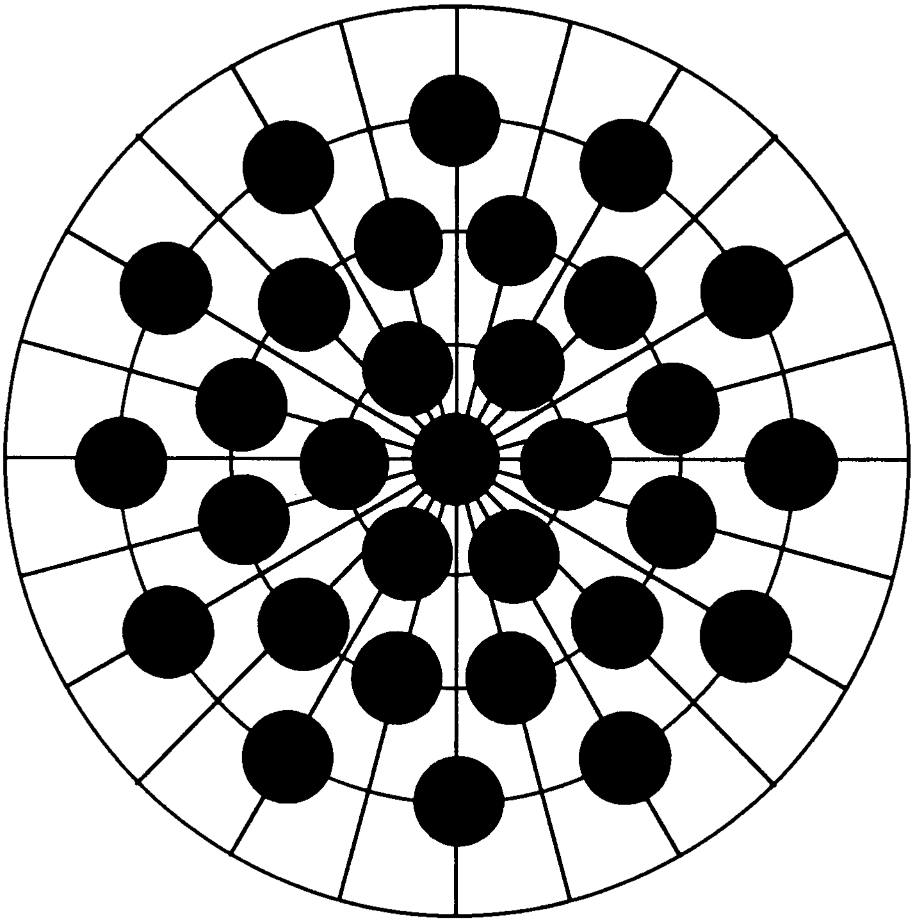

Figure 15. Injector pattern 3:6,12,12

Note: Figure is drawn to 250% scale.

APPENDIX B

MIXTURE RATIO DISTRIBUTIONS

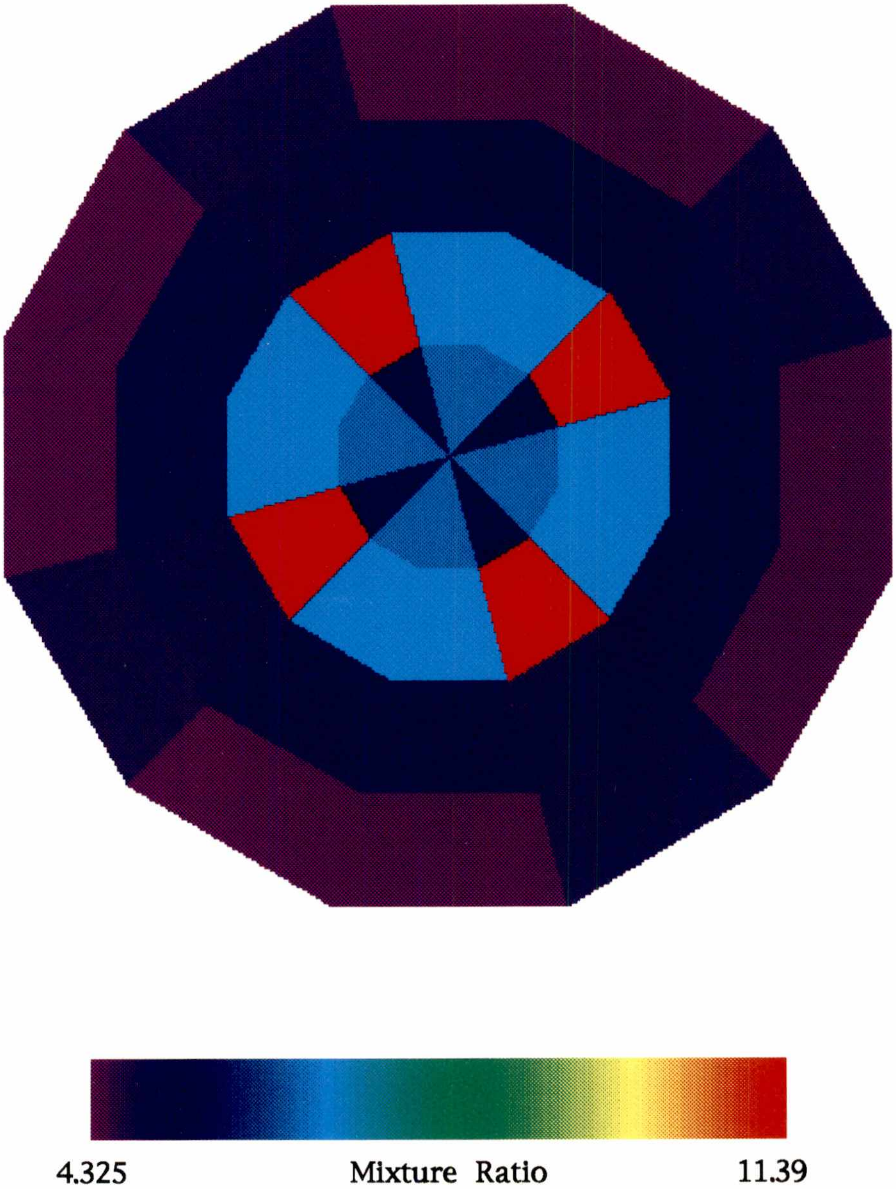

Figure 16. Unsmoothed mixture ratio distribution at the throat for pattern 2:4,8.

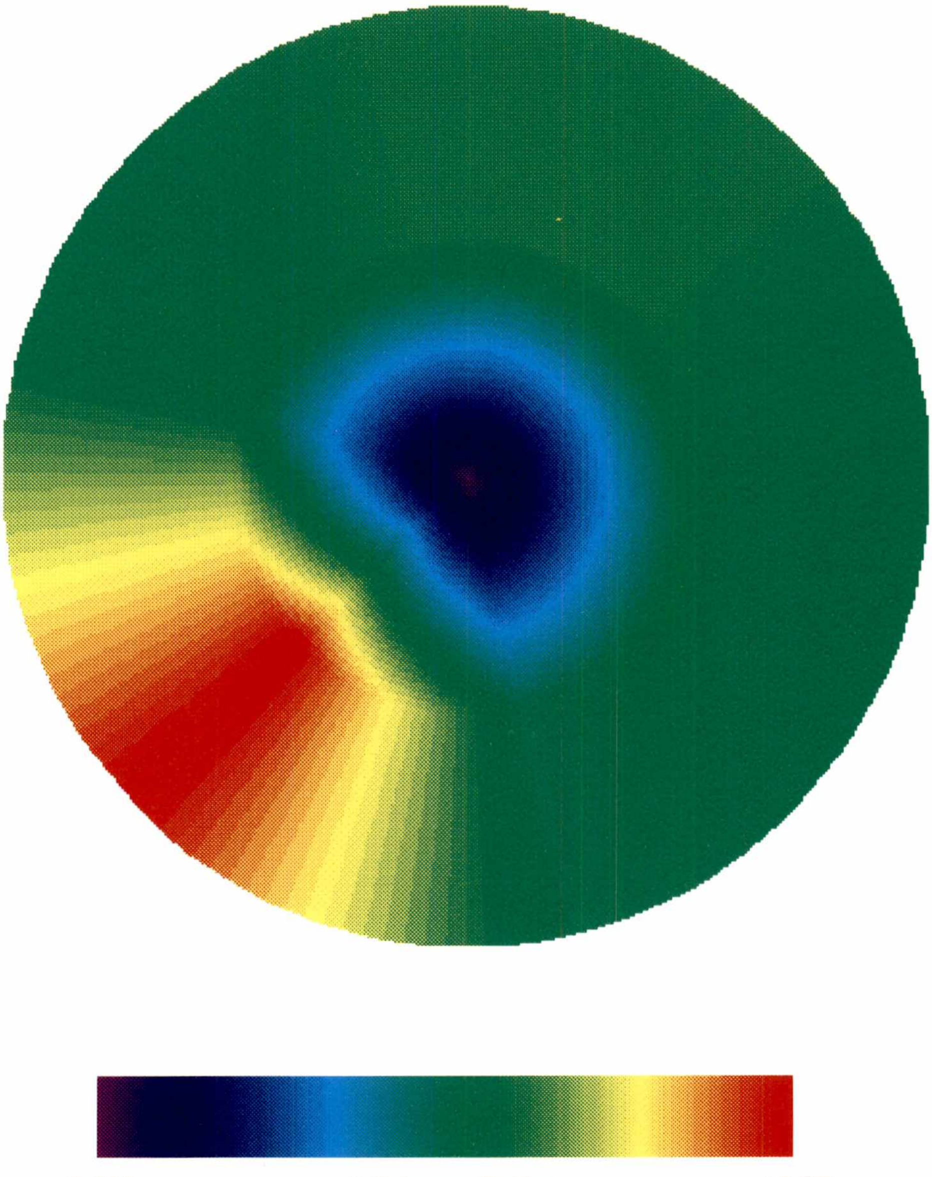

Figure 17. Mixture ratio distribution at the throat for pattern Sample.

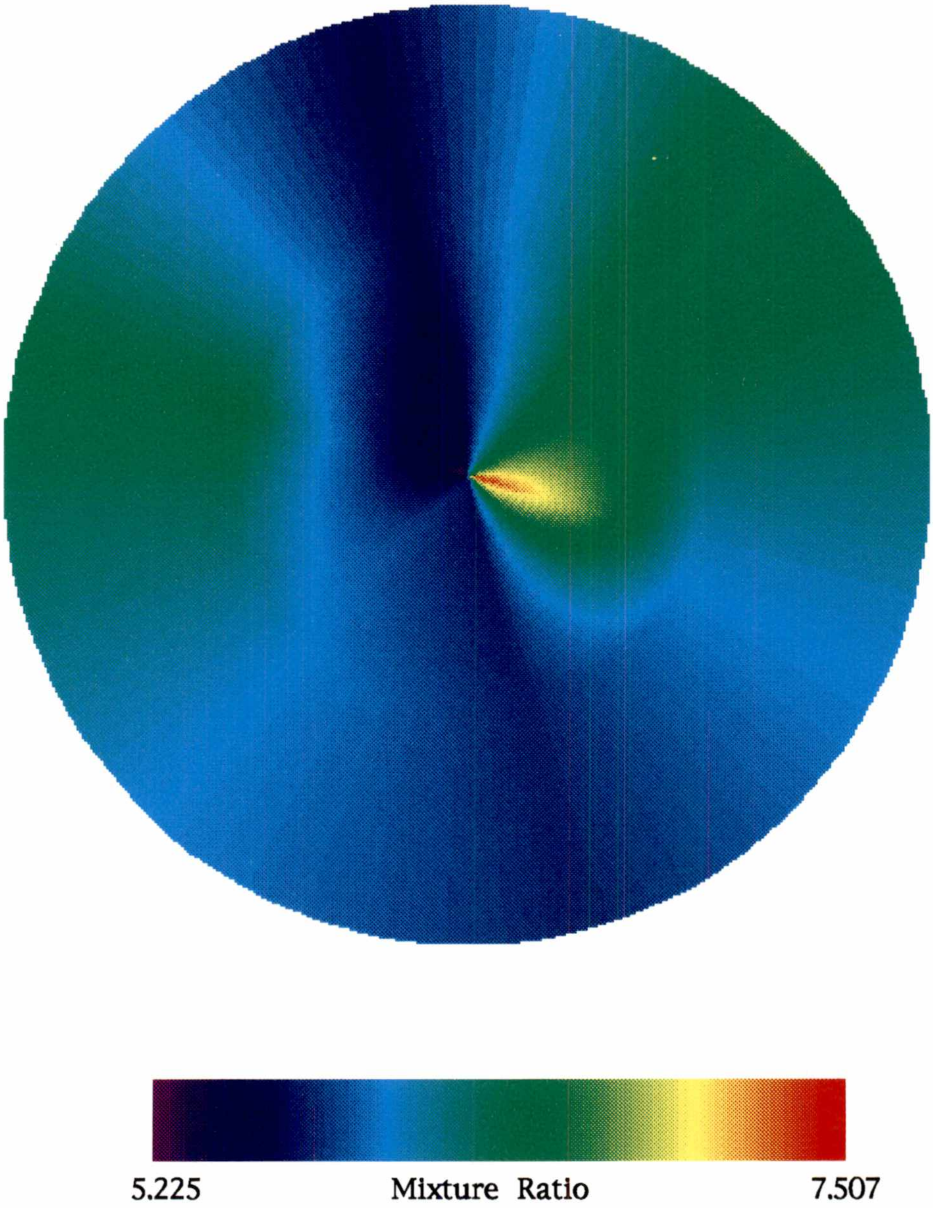

Figure 18. Mixture ratio distribution at the throat for pattern 1:7a.

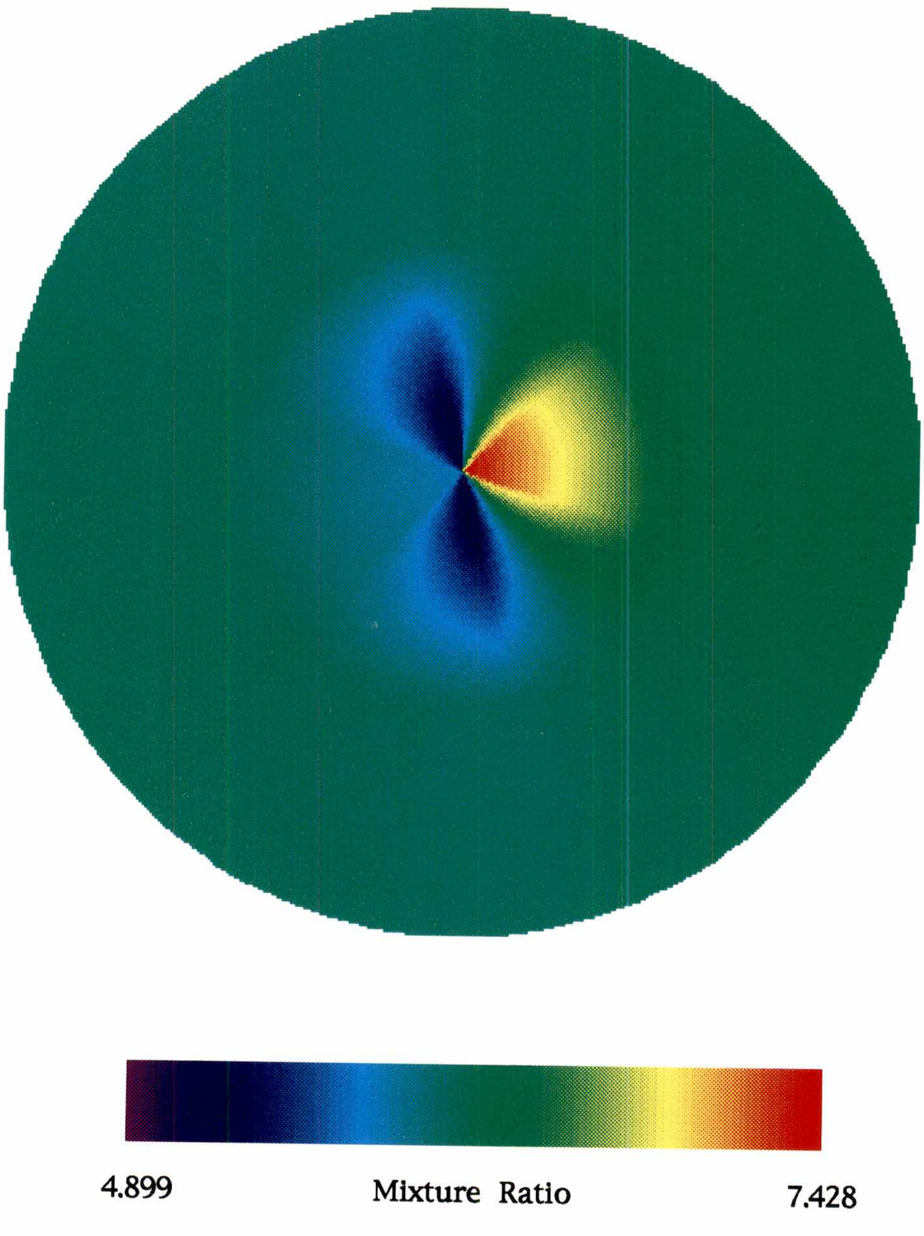

Figure 19. Mixture ratio distribution at the throat for pattern 1:7b.

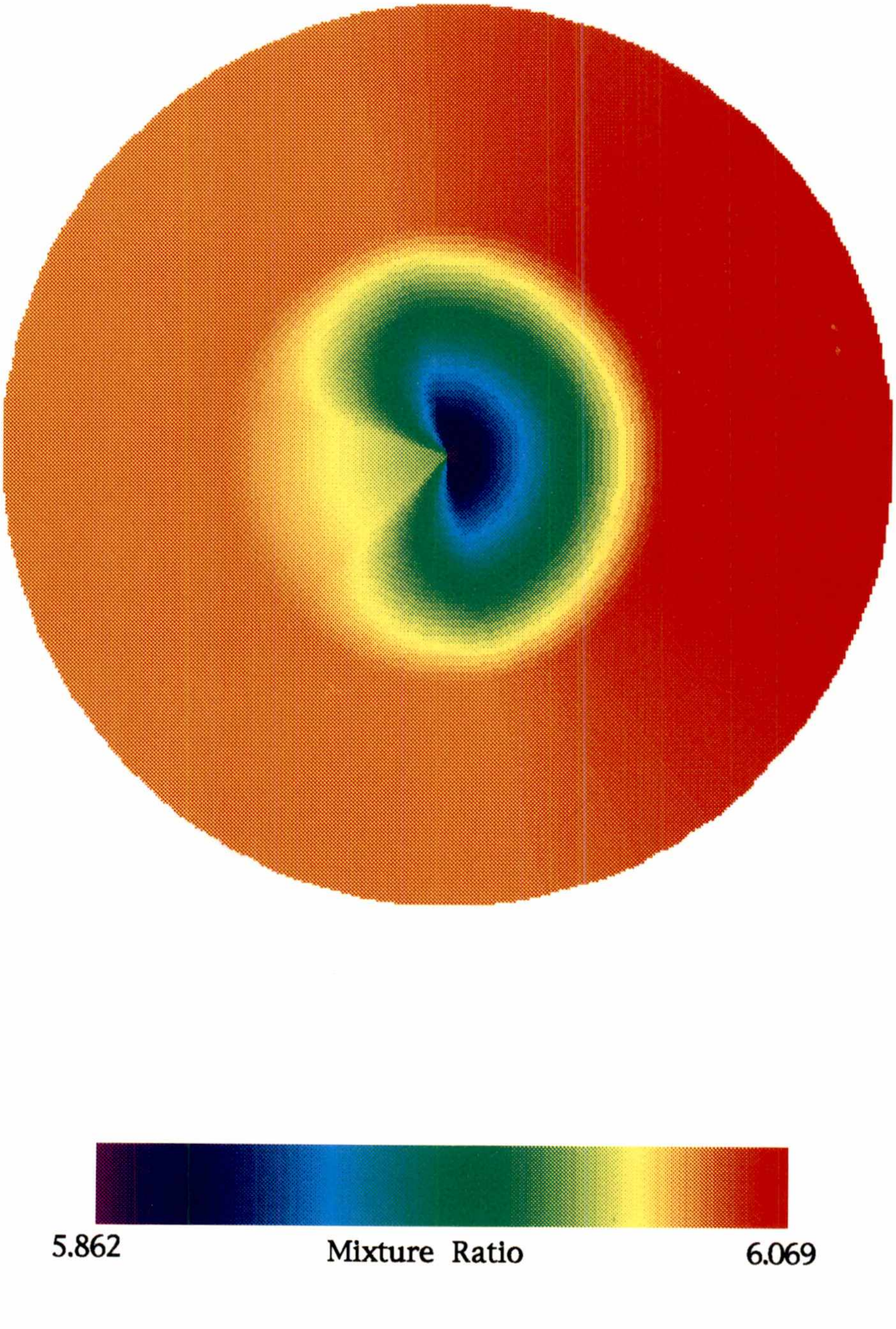

Figure 20. Mixture ratio distribution at the throat for pattern 1:7c.

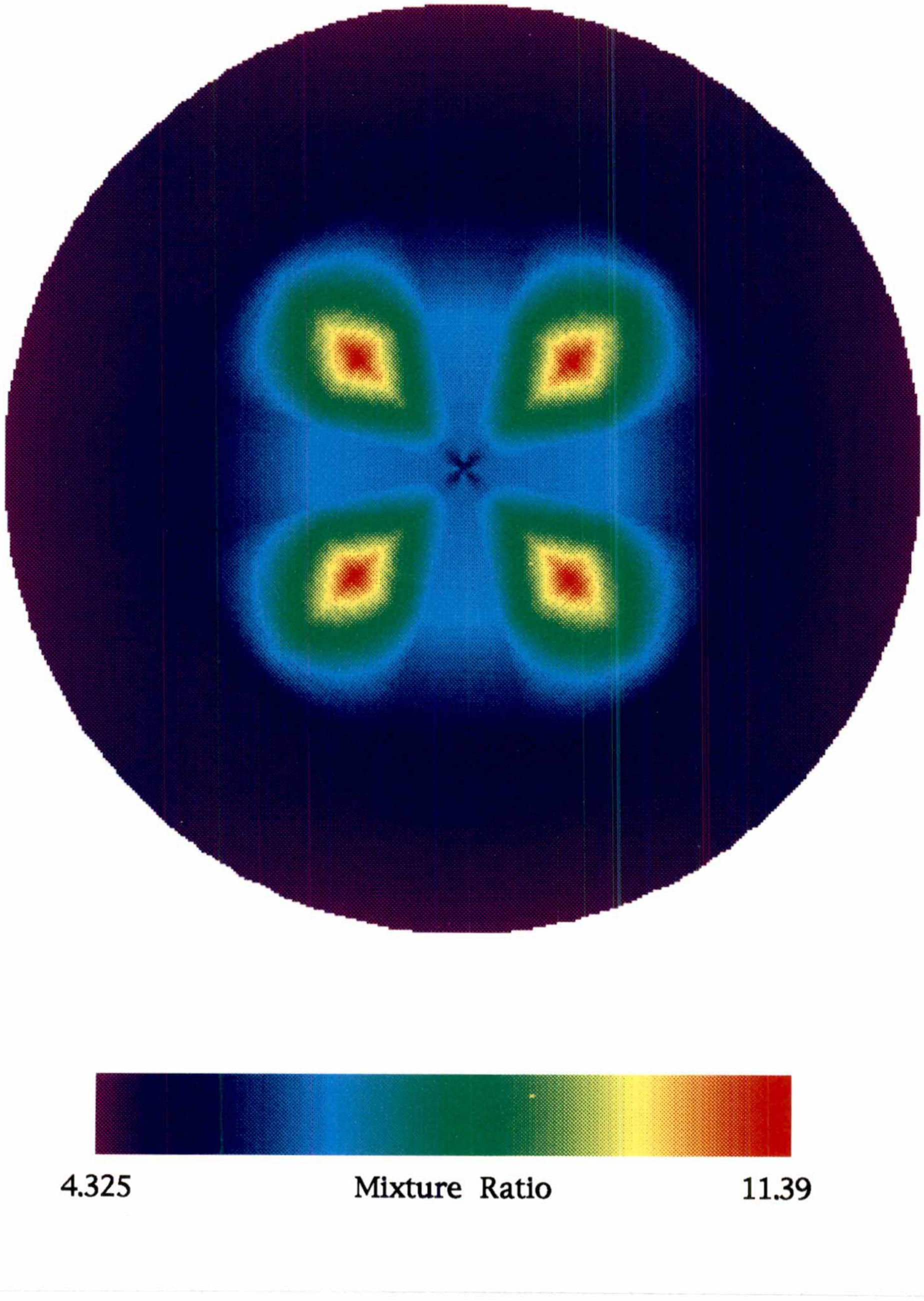

Figure 21. Mixture ratio distribution at the throat for pattern 2:4,8.

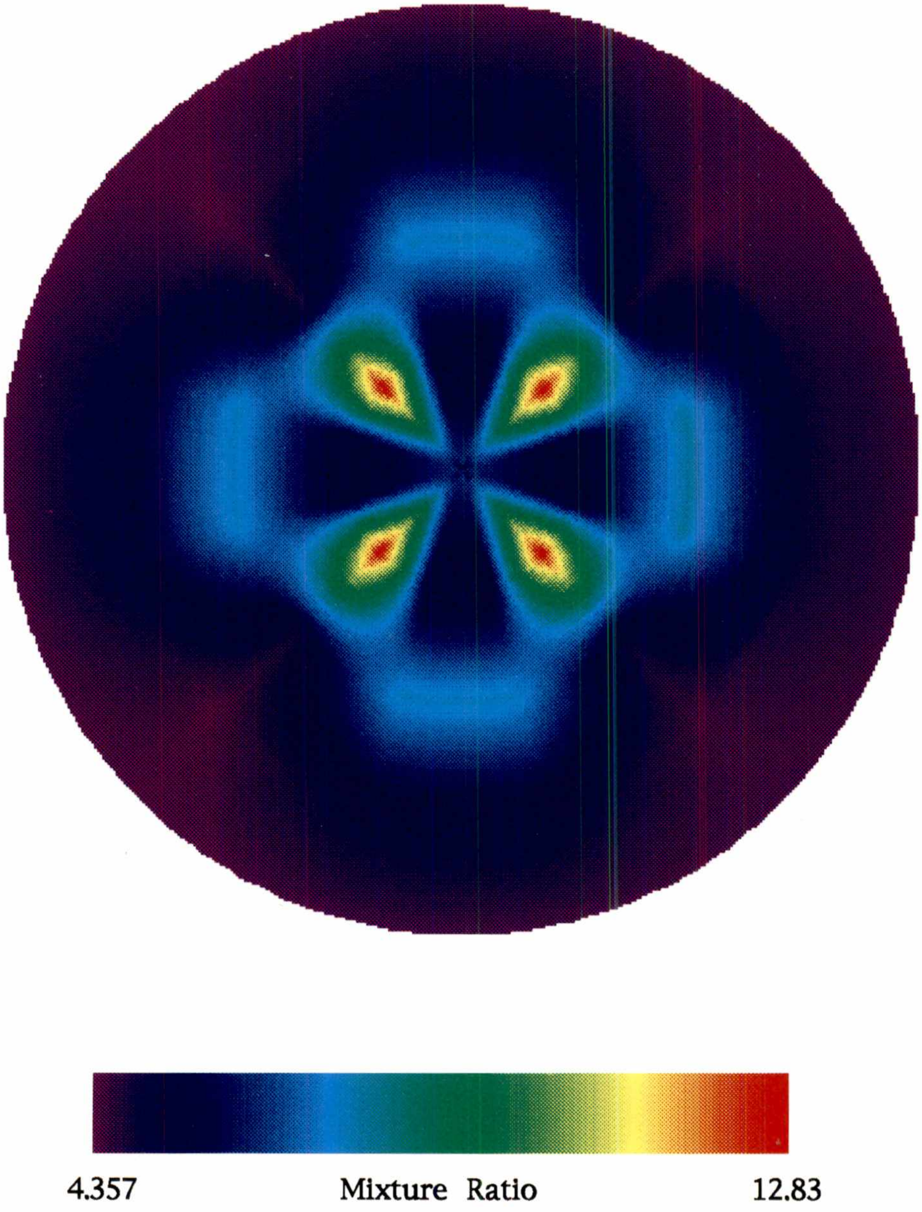

Figure 22. Mixture ratio distribution at the throat for pattern 3:4a.

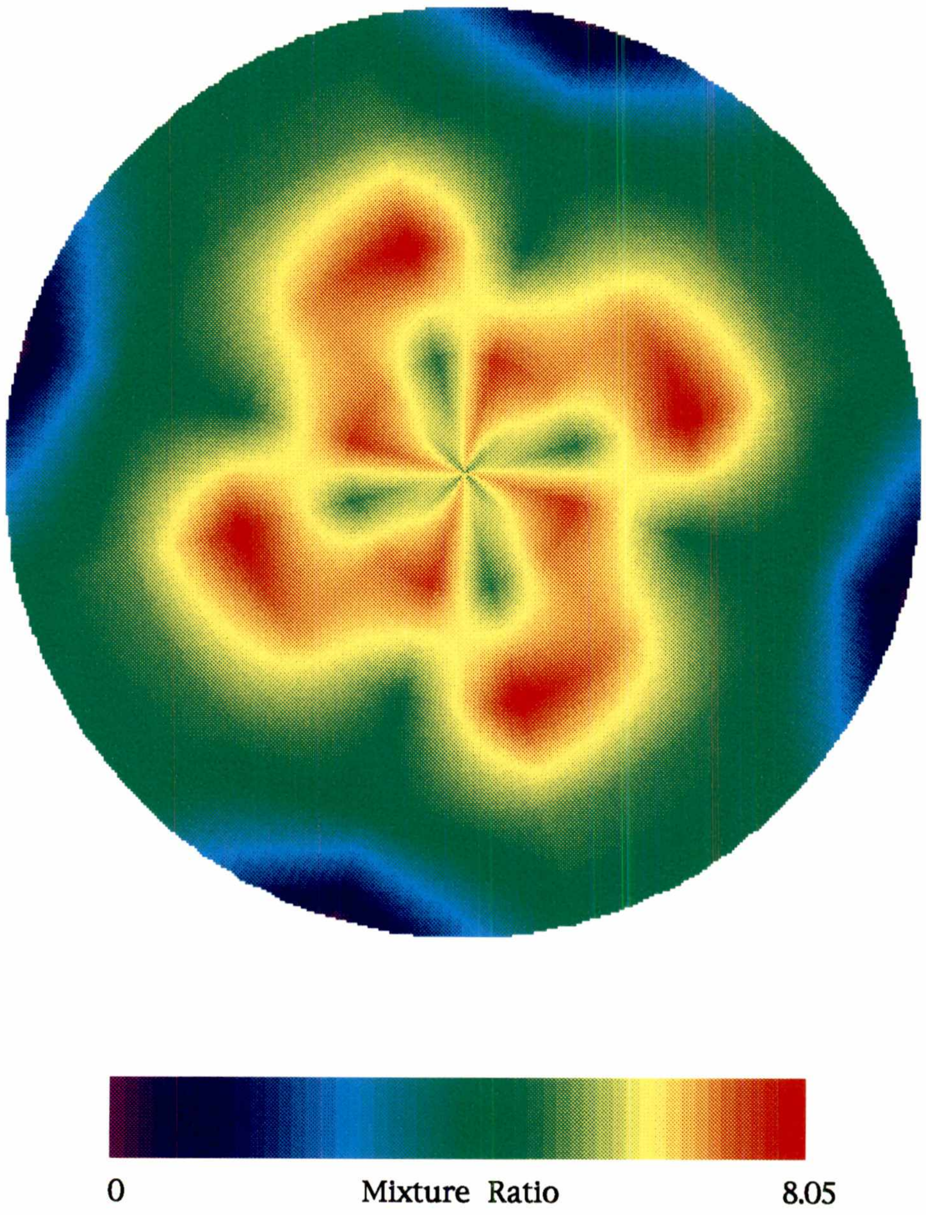

Figure 23. Mixture ratio distribution at the throat for pattern 3:4b.

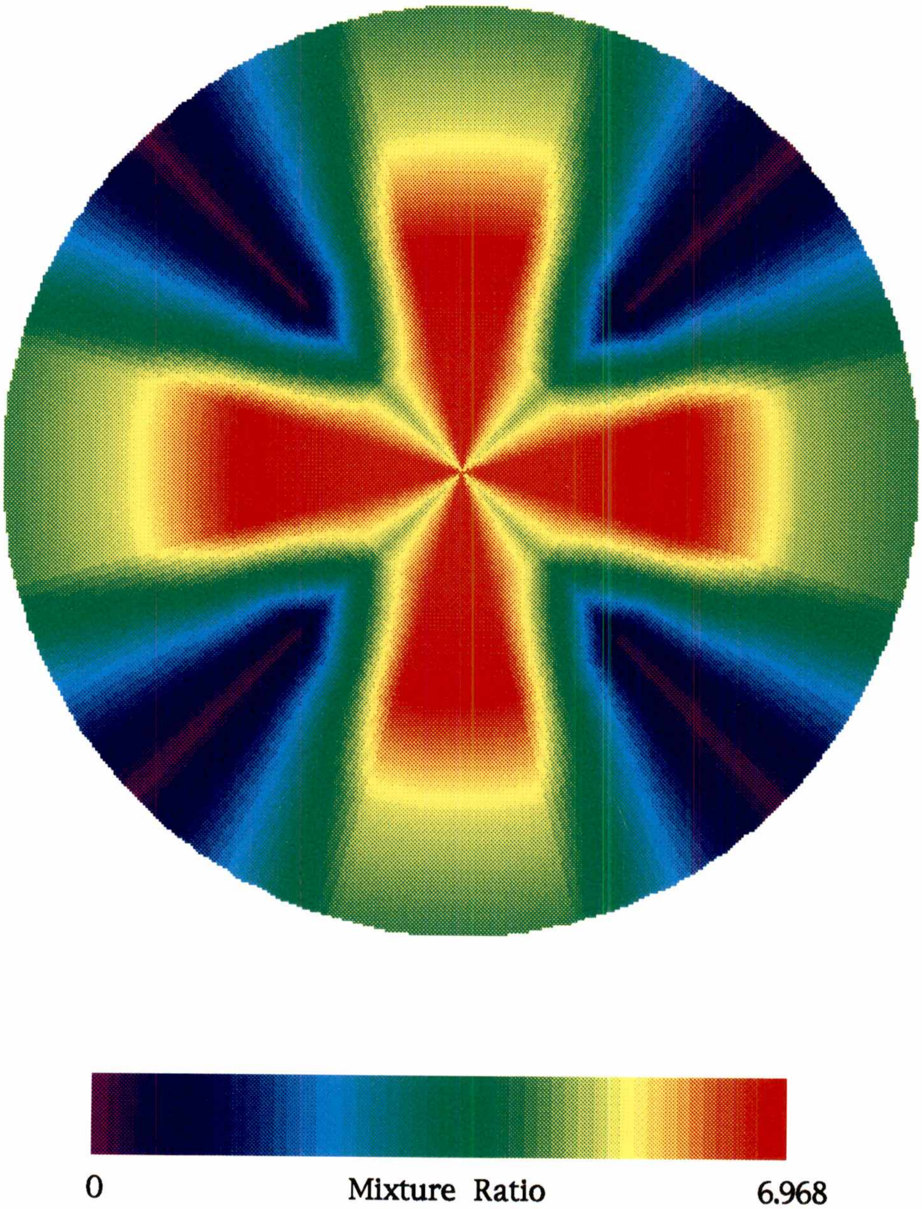

Figure 24. Mixture ratio distribution at the throat for pattern 3:4c.

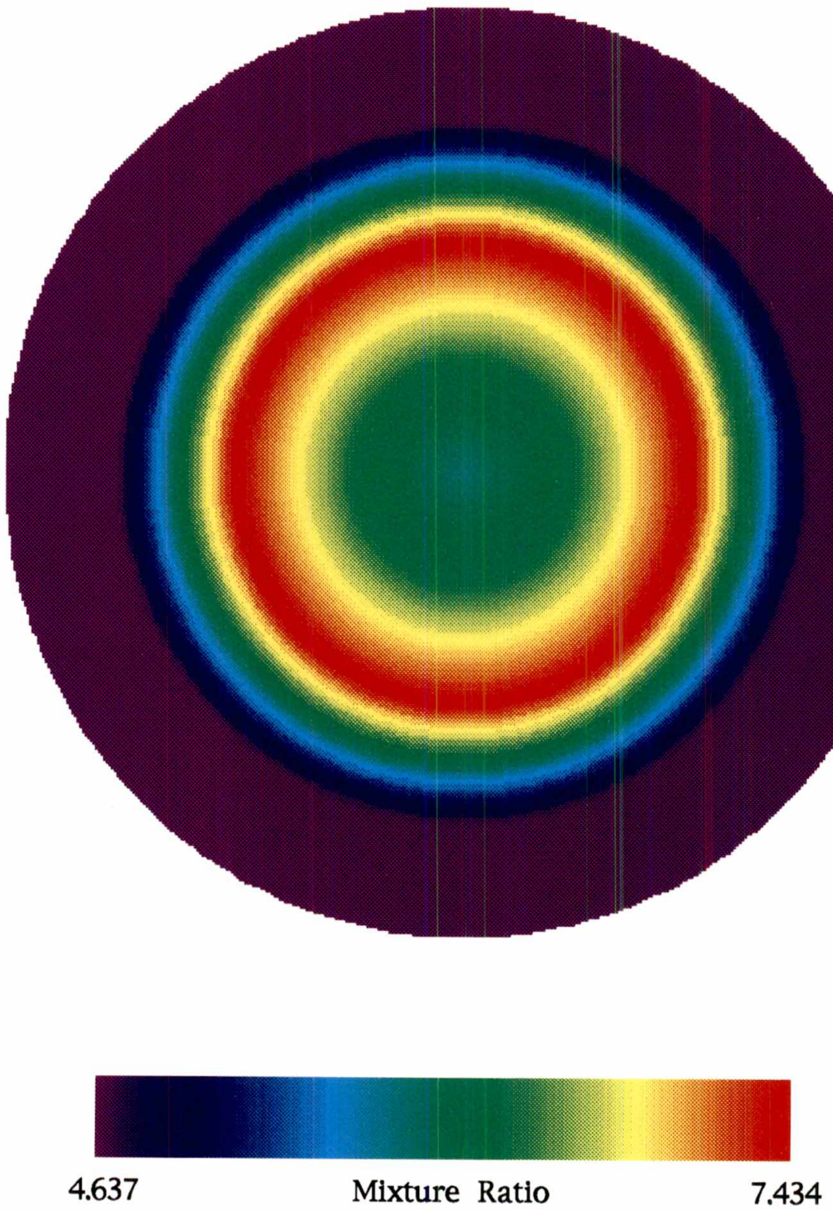

Figure 25. Mixture ratio distribution at the throat for pattern 3:6,12,12.

Vita

Nancy Diane O'Brien graduated from Selma High School in Selma, Alabama, in May, 1987. She entered Auburn University the following fall and graduated Magna Cum Laude with a Bachelor's of Science in Aerospace Engineering in August, 1991. She enrolled in The University of Tennessee Space Institute in the fall of 1991, studying aerospace engineering, focusing on space propulsion. She is presently employed by The University of Tennessee Space Institute as a graduate research assistant.